Cell Reports
Medicine

Article

Integrative metabolomics and transcriptomics identifies itaconate as an adjunct therapy to treat ocular bacterial infection

Graphical abstract

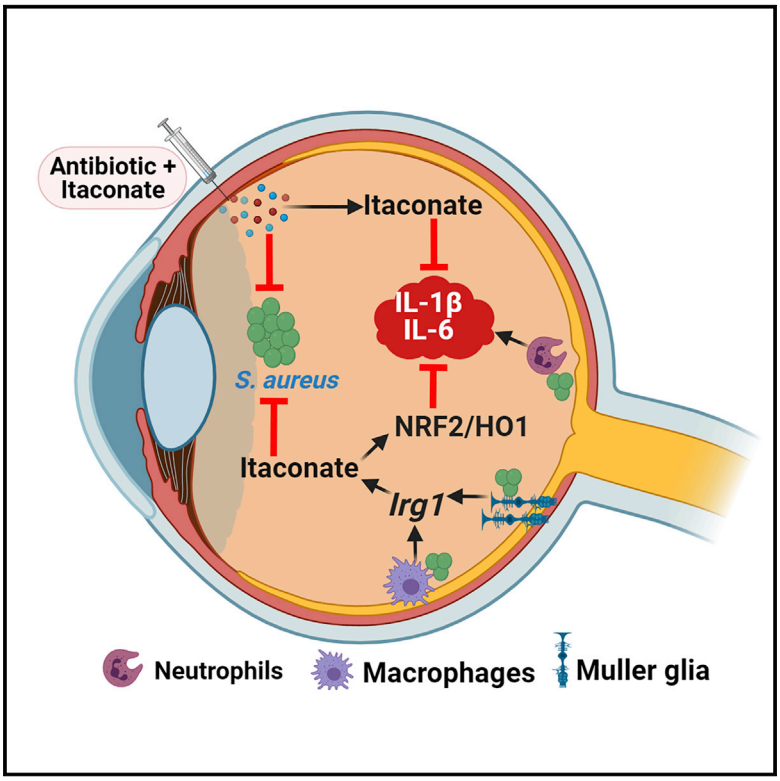

Authors

Sukhvinder Singh, Pawan Kumar Singh, Alokkumar Jha, Poonam Naik, Joveeta Joseph, Shailendra Giri, Ashok Kumar

Correspondence

akuma@med.wayne.edu

In brief

Eye infections remain the leading cause of blindness. Singh et al. show that the metabolite itaconate is produced in infected eyes to control aberrant inflammation. Itaconate exerts its anti-inflammatory effect by potentiating antioxidant NRF2/HO signaling and as an adjunct therapy reduces antibiotic dose required to treat ocular bacterial infection.

Highlights

- Bacterial infection increases *Irg1* and itaconate levels in the eye
- *Irg1* and *Nrf2* deficiency exacerbates intraocular bacterial infection
- Itaconate potentiates antioxidant NRF2/HO-1 signaling in the eye
- Itaconate treatment synergizes with antibiotics in ameliorating ocular infection

Singh et al., 2021, Cell Reports Medicine 2, 100277
May 18, 2021
https://doi.org/10.1016/j.xcrm.2021.100277

CellPress

Cell Reports Medicine

CellPress
OPEN ACCESS

Article

Integrative metabolomics and transcriptomics identifies itaconate as an adjunct therapy to treat ocular bacterial infection

Sukhvinder Singh,[1] Pawan Kumar Singh,[1] Alokkumar Jha,[2,3] Poonam Naik,[4] Joveeta Joseph,[4] Shailendra Giri,[5] and Ashok Kumar[1,6,7,*]

[1]Department of Ophthalmology, Visual and Anatomical Sciences, Kresge Eye Institute, Wayne State University School of Medicine, Detroit, MI, USA
[2]Cardiovascular Institute, Stanford University, Stanford, CA, USA
[3]Stanford Cancer Institute, Stanford University, CA, USA
[4]L.V. Prasad Eye Institute, Hyderabad, India
[5]Department of Neurology, Henry Ford Health System, Detroit, MI, USA
[6]Department of Biochemistry, Microbiology, and Immunology, Wayne State University School of Medicine, Detroit, MI, USA
[7]Lead contact
*Correspondence: akuma@med.wayne.edu
https://doi.org/10.1016/j.xcrm.2021.100277

SUMMARY

The eye is highly susceptible to inflammation-mediated tissue damage evoked during bacterial infection. However, mechanisms regulating inflammation to protect the eye remain elusive. Here, we used integrated metabolomics and transcriptomics to show that the immunomodulatory metabolite itaconate and immune-responsive gene 1 (*Irg1*) are induced in bacterial (*Staphylococcus aureus*)-infected mouse eyes, bone-marrow-derived macrophages (BMDMs), and Müller glia. Itaconate levels are also elevated in the vitreous of patients with bacterial endophthalmitis. *Irg1* deficiency in mice led to increased ocular pathology. Conversely, intraocular administration of itaconate protects both *Irg1*$^{-/-}$ and wild-type mice from bacterial endophthalmitis by reducing inflammation, bacterial burden, and preserving retinal architecture and visual function. Notably, itaconate exerts synergistic effects with antibiotics. The protective, anti-inflammatory effects of itaconate are mediated via activation of NRF2/HO-1 signaling and inhibition of NLRP3 inflammasome. Collectively, our study demonstrates the *Irg1*/itaconate axis is a regulator of intraocular inflammation and provides evidence for using itaconate, along with antibiotics, to treat bacterial infections.

INTRODUCTION

The incidence of intraocular infections, such as bacterial endophthalmitis, is on the rise because of a growing elderly population, which has increased the demand for eye surgeries to treat diseases such as cataracts, age-related macular degeneration (AMD), and glaucoma.[1,2] Treatment for each of these conditions, along with the widespread use of intravitreal injections to manage neovascular AMD and diabetic retinopathy, predisposes individuals to endophthalmitis.[3–5] The current treatment for bacterial endophthalmitis involves the intravitreal injection of antibiotics[6] that eliminates the bacteria but fails to suppress inflammation-mediated ocular tissue damage and often results in partial or complete loss of vision.[7,8] Thus, host-directed therapeutics are needed to complement pathogen-targeted approaches to treat ocular infections.

Transcriptomic and metabolomic analyses are powerful high-throughput technologies that have been increasingly used to uncover disease mechanisms and biomarkers,[9] including several pathways involved in the pathobiology of ocular infections.[10–12] These analyses have revealed a connection between energy metabolism and ocular innate immunity in bacterial[13] and viral infections.[14,15] Specifically, in bacterial endophthalmitis, the cellular metabolism of both residential (e.g., microglia) and infiltrating cells (e.g., neutrophils and macrophages) exhibited increased glycolysis.[13] Inhibiting glycolysis in bacterial endophthalmitis attenuates intraocular inflammation,[14] suggesting a mechanism that can be targeted for the treatment of ocular infections. Thus, these pre-clinical studies have identified potential mechanisms that enhance protective pathways or limit destructive host responses to attenuate inflammation from bacterial infection in the eye.

In our transcriptomic data from the mouse retina after *Staphylococcus aureus* infection,[10] we observed marked upregulation of the immune responsive gene 1 (*Irg1*), which is also called *Acod1*. Under inflammatory conditions, *Irg1* drives the production of itaconate, a product of the Krebs cycle intermediate *cis*-aconitate and has profound immunomodulatory properties.[16] Expression of *Irg1* and the subsequent production of itaconate are increased in response to lipopolysaccharide (LPS) challenge[17,18] or bacterial[19] and viral infections.[18,20] *Irg1* is essential for neutrophil infiltration, limiting immune-mediated tissue

damage in *Mycobacterium tuberculosis* (*Mtb*) infection,[21] and promoting trained immunity.[22] In contrast, *Irg1* deficiency in immune cells results in reduced antimicrobial activities.[23] The antibacterial properties of itaconate are due to its ability to inhibit isocitrate lyase, a bacterial glyoxylate shunt enzyme. Moreover, it inhibits bacterial growth at supraphysiological concentrations[24–26] and is predicted to be an inflammatory marker.[24,27] Thus, because of its broad immunomodulatory properties, the *Irg1*/itaconate axis[28] has recently become an active area of investigation in the field of immunometabolism.

To determine alterations in gene expression and metabolic pathways that occur during bacterial endophthalmitis, we performed transcriptomic and metabolomic analyses of retinal tissue from infected mouse eyes and the vitreous of patients with bacterial endophthalmitis, which showed increased levels of itaconate. Based on these observations, we hypothesized that the production of itaconate is a protective host response in the eye during bacterial infections. Using *Irg1*$^{-/-}$ mice and itaconate analogs, we show that *Irg1*/itaconate protects the eye from bacterial endophthalmitis by resolving inflammation. In addition, activation of the *Irg1*/itaconate pathway enhanced the NRF2/HO1 antioxidant pathway, which abrogates inflammation and reduces retinal cell death. Moreover, itaconate synergized with antibiotics to limit bacterial growth and potentiate anti-inflammatory/antioxidant pathways to prevent tissue damage.

RESULTS

Irg1/Itaconate pathway is upregulated in bacterial endophthalmitis

In the present study, we integrated metabolomic and transcriptomic approaches to identify key metabolites, genes, and pathways altered during bacterial endophthalmitis. Using retinal tissue from uninfected or *S.-aureus*-infected mouse eyes at different time points after infection, we performed temporal metabolomic and transcriptomic analyses. Principal component analysis (PCA) of untargeted metabolomics showed distinct clustering of various experimental groups, suggesting alterations in metabolite profiles among the different time points (Figure 1A). To identify differentially produced metabolites across various time points with respect to controls, we used a partial least-squares discriminant analysis (PLS-DA), in which each group was divided into a two-dimensional score plot with two principal components (variance of 46.71%). To show the differentially altered metabolites from the PCA analysis, we listed the top 25 metabolites using variable importance in projection (VIP) scores, with the top five metabolites being biopterin, *N*-acetyl-β-D-glucosamine, itaconate, *N*-acetylaspartic acid, and nicotinamide mononucleotide, respectively (Figure 1B). Because of the variability in the experimental groups, we reaffirmed the capability classification of these top altered metabolites by applying the data to a random forest classification model, which showed a prediction error rate of the top metabolites to be less than 8.2% (Figure 1C). Itaconate was the top altered metabolite identified by this model, confirming its classification as one of the metabolites most affected upon *S. aureus* infection (Figure 1D).

To identify the genes associated with altered metabolic pathways, we analyzed transcriptomic data obtained from the retinas of *S. aureus*-infected mice at 6, 12, and 24 h and retinas of the uninfected control eyes. Among the top 100 differentially expressed genes (DEGs), 63 were differentially expressed across all three time points (Figure 1E). A heatmap of these DEGs shows the differential changes in expression across the three time points, with *Irg1* having the highest variability (Figure 1F). Given the relationship between *Irg1* and itaconate, we correlated the top 63 DEGs and the top 10 altered metabolites and extracted a correlation score for "itaconate" and "*Irg1*," which we plotted in a pairs plot with each of the three time points (6, 12, and 24 h; Figures S1A and S1B). This analysis revealed a positive correlation between itaconate and *Irg1*. Collectively, our integrated omics analysis revealed that itaconate and *Irg1* have the highest concurrent variability across all time points in the context of *S. aureus* endophthalmitis.

Bacterial infection increases *Irg1* and Itaconate levels in mouse and human eyes

Although our transcriptomic and metabolomic analyses showed upregulation of *Irg1* and elevated levels of itaconate in infected eyes, the functional relevance of this pathway is unknown in bacterial endophthalmitis. Therefore, we performed a time-course study using a mouse model of *S. aureus* endophthalmitis and cultured cells to validate our multi-omics findings. Our data showed a time-dependent increase in the expression of *Irg1* at both the mRNA (Figure 2A) and protein (Figure 2B) levels in *S. aureus*-infected mouse retinas. Macrophages are one of the major populations of innate immune cells infiltrating the eye during infection; therefore, we used bone marrow-derived macrophages (BMDMs) and observed a similar increase in *Irg1* expression after *S. aureus* infection in cultured wild-type (WT) BMDMs (Figures 2C and 2D) and in the human retinal Müller glia cell line MIO-M1, which are the residential glial cells of the retina (Figures 2E and 2F). Because *S. aureus* produces several virulence factors that contribute toward the pathogenesis of endophthalmitis,[29] we sought to determine their effects on *Irg1* expression. Our results show that, in addition to live *S. aureus*, heat-killed *S. aureus* (HK), lipoteichoic acid (LTA), and peptidoglycan (PGN), but not the α-toxin or toxic shock syndrome toxin-1 (TSST-1), induced the *Irg1* expression both at transcript (Figure 2G) and protein (Figure 2H) levels. Because *Irg1* is responsible for the synthesis of itaconate during the Krebs cycle (Figure 2I), we used a targeted metabolomics approach to measure itaconate levels after *S. aureus* infection. Consistent with induced *Irg1* expression, the levels of itaconate were noticeably increased in *S. aureus*-infected mouse vitreous/retinal tissue (Figure 2J) as well as in BMDMs (Figure 2K).

To determine whether itaconate is also produced during ocular bacterial infection in humans, we assessed itaconate levels in the vitreous samples from 22 patients who were clinically diagnosed with endophthalmitis, which was confirmed by a positive bacterial culture. The vitreous samples (n = 10) from patients who underwent vitrectomy for other retinal diseases (e.g., retinal detachment) were used as healthy controls (HC). Detailed patient demographics are provided in Table S1. Targeted metabolomics analyses revealed elevated levels of itaconate in the vitreous of patients with bacterial endophthalmitis compared with HC, although no significant difference was

CellPress
OPEN ACCESS

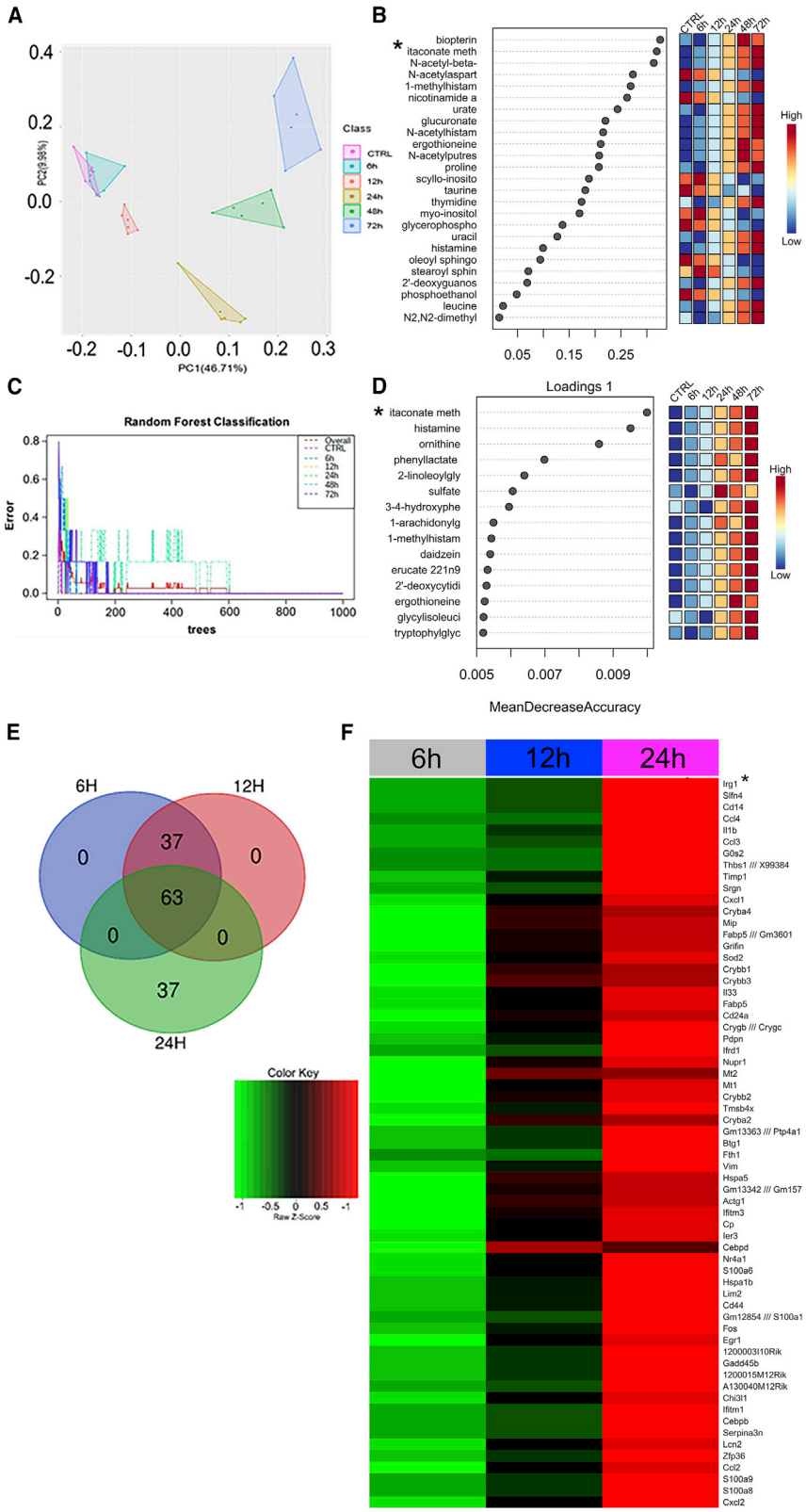

Figure 1. Metabolomic and transcriptomic profiling reveals upregulation of *Irg1* and increased itaconate production in mouse eyes during bacterial endophthalmitis

(A–D) Endophthalmitis was induced in C57BL/6 (B6) WT mice (n = 6 per time point: 6, 12, 24, 48, and 72 h) by intravitreal inoculation of *S. aureus* RN6390 (5,000 CFUs/eye). Eyes injected with PBS were used as controls. At the indicated time points, the retinas were harvested and subjected to untargeted metabolomics analysis. (A) Principal component (PC) of untargeted metabolomics data at indicated time points. (B) Top 25 altered metabolites based on VIP scores. (C) Random forest classification model and error identification model to validate the top altered metabolites. (D) Top 15 metabolites that were differentially altered across the various time points, as identified by random forest classification. (E and F) In another set of experiments, endophthalmitis was induced in B6 WT mice (n = 3 at each time point), and retinas were harvested at 6, 12, and 24 h after infection. Eyes with PBS injection were used as controls. Total RNA was extracted from control and infected retinas and subjected to microarray for transcriptomic profiling. (E) Venn diagram representing differentially expressed genes (DEGs). (F) Heatmap of 63 common genes.
See also Figure S1.

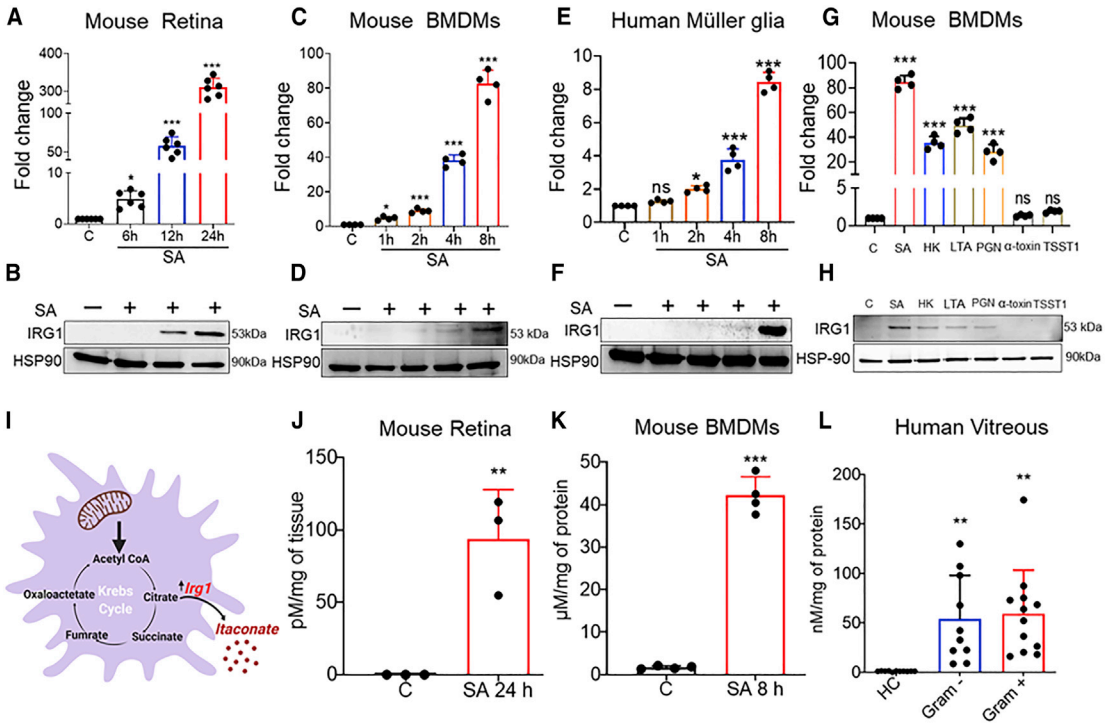

Figure 2. IRG1 expression and itaconate production are induced in mouse and human eyes during bacterial endophthalmitis

(A and B) Endophthalmitis was induced in the eyes of B6 WT mice (n = 6 per time point) by intravitreal inoculation of *S. aureus* (SA) RN6390 (5,000 CFUs/eye). PBS-injected eyes were used as controls. At the indicated time points post-infection, eyes were enucleated, and retinal tissue was used to quantitate *Irg1* expression by qPCR (A) and western blot (B), normalized with β-actin and heat shock protein 90 (HSP90) as endogenous controls, respectively.

(C and D) BMDMs from WT mice (n = 4/condition) were challenged with *S. aureus* (multiplicity of infection [MOI] 10:1) for the indicated time points. *Irg1* expression was measured by qPCR (C) and western blot (D), normalized with β-actin and HSP90 as endogenous controls, respectively.

(E and F) Human retinal Müller glia cell line, MIO-M1, (n = 4/condition) was infected with *S. aureus* (MOI 10:1) for the indicated time points. *Irg1* expression was measured by qPCR (E) and western blot (F), normalized with β-actin and HSP90 as endogenous controls, respectively.

(G and H) BMDMs from WT mice (n = 4/condition) were challenged with *S. aureus* (SA), heat-killed SA (HK), staphylococcal lipoteichoic acid (LTA), peptidoglycan (PGN), α-toxin, and, toxic shock syndrome toxin 1 (TSST1) for 8 h. *Irg1* expression was measured by qPCR (G) and western blot (H), normalized with β-actin and HSP90 as endogenous controls, respectively.

(I) Schematic showing the role of *Irg1* in itaconate production.

(J–L) Itaconate estimation by liquid chromatography-mass spectrometry (LC-MS). (J) retinal tissue from WT mice 24 h after *S. aureus* infection (n = 3, six retinas pooled per sample) or PBS-injected control eyes (C; n = 3);

(K and L) BMDMs 8 h after *S. aureus* infection (K; n = 4); and (L) vitreous samples from patients with Gram-negative ($Gram^-$; n = 10) and Gram-positive ($Gram^+$; n = 12) bacterial endophthalmitis or healthy controls (HCs; n = 10).

The data represented are the culmination of two independent experiments and are shown as means ± SD. Statistical analysis was performed using one-way ANOVA (panels A, C, E, G, and L) or unpaired t test (J and K). ns; non-significant, *p < 0.05, **p < 0.001, ***p < 0.0001. See also Table S1.

observed in the itaconate levels of those infected with Gram-positive (mean ± SD, 50.56 ± 13.04 nM) versus Gram-negative (mean ± SD, 63.23 ± 13.24 nM) bacteria (Figure 2L; Table S1). These results show that *Irg1* expression is induced and itaconate levels are elevated in mouse and human eyes upon infection, indicating a potential role for the *Irg1*/itaconate signaling in the pathobiology of bacterial endophthalmitis.

IRG1 deficiency exacerbates bacterial endophthalmitis

To investigate the role of IRG1 and itaconate in ocular infection, we induced *S. aureus* endophthalmitis in WT and $Irg1^{-/-}$ mice. We previously showed that WT mouse eyes challenged with an infective dosage of 500 colony forming units (CFUs) of *S. aureus* resolve the infection within 48–72 h (resolving condition), whereas a dosage of 5,000 CFUs causes severe endophthalmitis (non-resolving condition) leading to blindness.[13,30] Thus, the bacterial dosage is an important determinant in disease outcomes in endophthalmitis.[31,32] Given the anti-inflammatory role of *Irg1*/itaconate, we hypothesized that IRG1 deficiency would delay the resolution of inflammation and worsen disease outcomes. As such, we decided to assess the effects of the 500 CFUs/eye dosage, which is typically resolved in WT mice. In comparison to WT mice, endophthalmitis was exacerbated in $Irg1^{-/-}$ mice, as demonstrated by increased corneal haze, opacity, and hypopyon (Figure 3A, top panel). Histopathological analysis showed increased retinal tissue damage, retinal folding, and heavy cellular infiltrate in the eyes of $Irg1^{-/-}$ mice (Figure 3A, bottom panel), and this was associated with reduced retinal function as determined by electroretinography (ERG) showing a decline in a- and b-wave amplitudes (Figure 3B). Moreover,

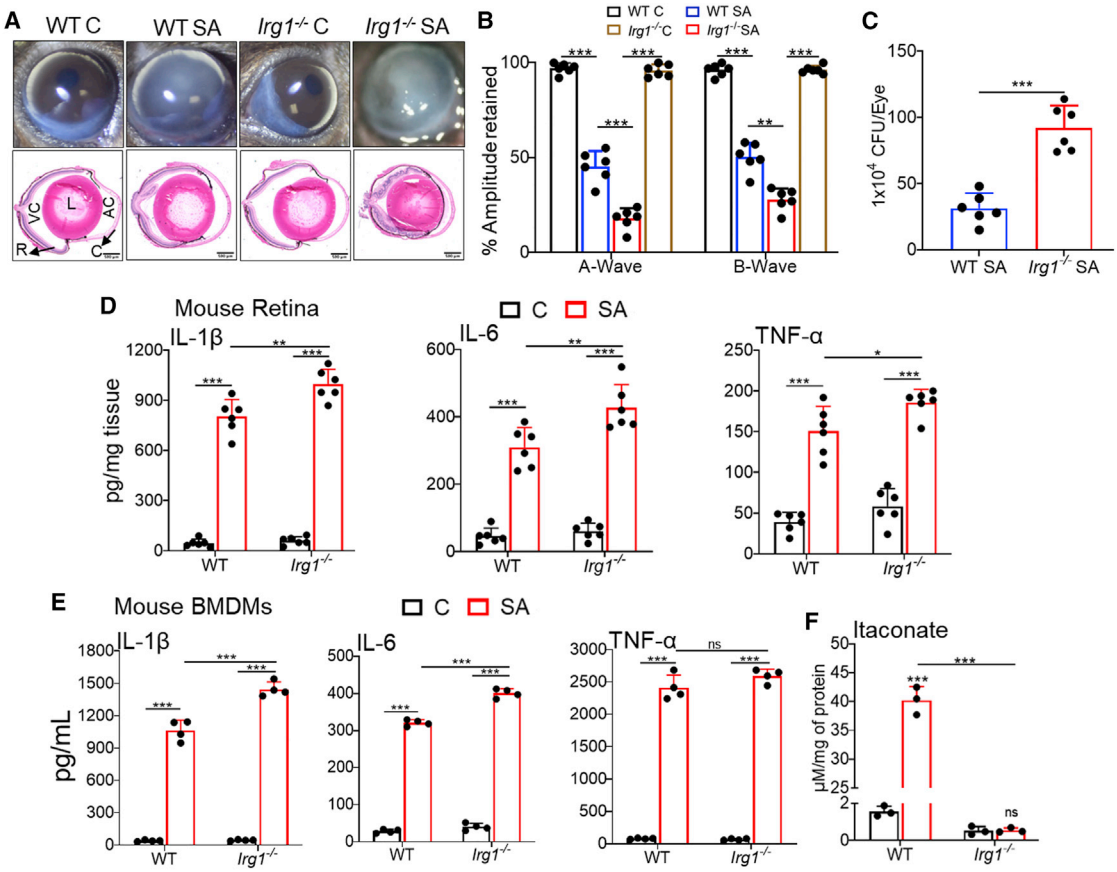

Figure 3. *Irg1*$^{-/-}$ mice exhibit exacerbated bacterial endophthalmitis

(A–D) Endophthalmitis was induced in the eyes of B6 WT and *Irg1*$^{-/-}$ mice (n = 6) by intravitreal inoculation of *S. aureus* (SA) RN6390 (500 CFUs/eye). Eyes in WT (WT C) and *Irg1*$^{-/-}$ (*Irg1*$^{-/-}$ C) mice with PBS injection were included as controls. (A, top panel) Representative slit-lamp micrograph showing corneal haze/opacity at 48 h post-infection (hpi). (A, bottom panel) H&E staining of eyes that were enucleated at 48 hpi for histopathological analysis. (B) The percentage of a- and b-wave amplitudes from scotopic ERG that were recorded from *S. aureus*-infected WT and *Irg1*$^{-/-}$ mice (n = 6 for each group) and compared with PBS-injected control eyes whose wave amplitudes were adjusted to 100%. (C) The intraocular bacterial burden in eye lysates from mice treated in (A) was determined by serial dilution and plate count method and represented as CFUs/eye (n = 6) (D) The indicated inflammatory cytokines in whole eye lysates were quantified by ELISA.

(E) WT and *Irg1*$^{-/-}$ BMDMs (n = 4/condition) were either left uninfected 'C' or infected with *S. aureus* RN6390 'SA' (MOI 10:1) for 8 h. The inflammatory cytokines (IL-1β, IL-6, and TNF-α) were quantified from the conditioned media by ELISA.

(F) Itaconate levels in WT and *Irg1*$^{-/-}$ BMDMs (n = 3) that were infected with *S. aureus* (MOI 10:1) for 8 h and quantified by LC-MS.

The data represented are the culmination of two to three independent experiments and are shown as means ± SD. Statistical analysis was performed using two-way ANOVA (panels B, D, E, and F) with Tukey's multiple comparison test or by unpaired t test (panel C). ns; non-significant, *p < 0.05, **p < 0.001, ***p < 0.0001. C, cornea; AC, anterior chamber; L, lens; VC, vitreous chamber; R, retina. See also Figure S2.

the intraocular bacterial burden (Figure 3C) was significantly higher in *Irg1*$^{-/-}$ mice with respect to their WT counterparts, which coincided with elevated levels of the inflammatory mediators, interleukin 1 beta (IL-1β), IL-6, and tumor necrosis factor alpha (TNF-α) (Figure 3D). The anti-inflammatory role of *Irg1* in response to *S. aureus* infection was also confirmed in BMDMs isolated from *Irg1*$^{-/-}$ mice, which showed increased levels of inflammatory mediators (Figure 3E). The effect of *Irg1* deficiency on itaconate production was revealed by drastically low levels of itaconate in *Irg1*$^{-/-}$ BMDMs (Figure 3F). Together, these findings indicate that *Irg1* exerts protective effects in the eye by reducing intraocular inflammation.

To determine whether the increased susceptibility of *Irg1*$^{-/-}$ mice to bacterial endophthalmitis at an even lower infectious dose of *S. aureus* was due to defective production of itaconate, we performed a rescue experiment; in which, *Irg1*$^{-/-}$ mice were supplemented with 4-octyl itaconate (OI), an itaconate derivative, via intravitreal injection 6 h after *S. aureus* infection (Figure S2A). Mice that received OI had reduced corneal haze/opacity and hypopyon, and histopathological analysis showed the retinal architecture was preserved (Figure S2B). ERG analysis showed that itaconate treatment significantly retained a- and b-wave amplitudes as compared with the untreated disease group (Figure S2C). Similarly, the bacterial burden (Figure S2D) and inflammatory cytokines (Figure S2E) were significantly reduced in itaconate-treated eyes. These results indicate that exogenous supplementation of itaconate protected *Irg1*$^{-/-}$ mice from bacterial endophthalmitis.

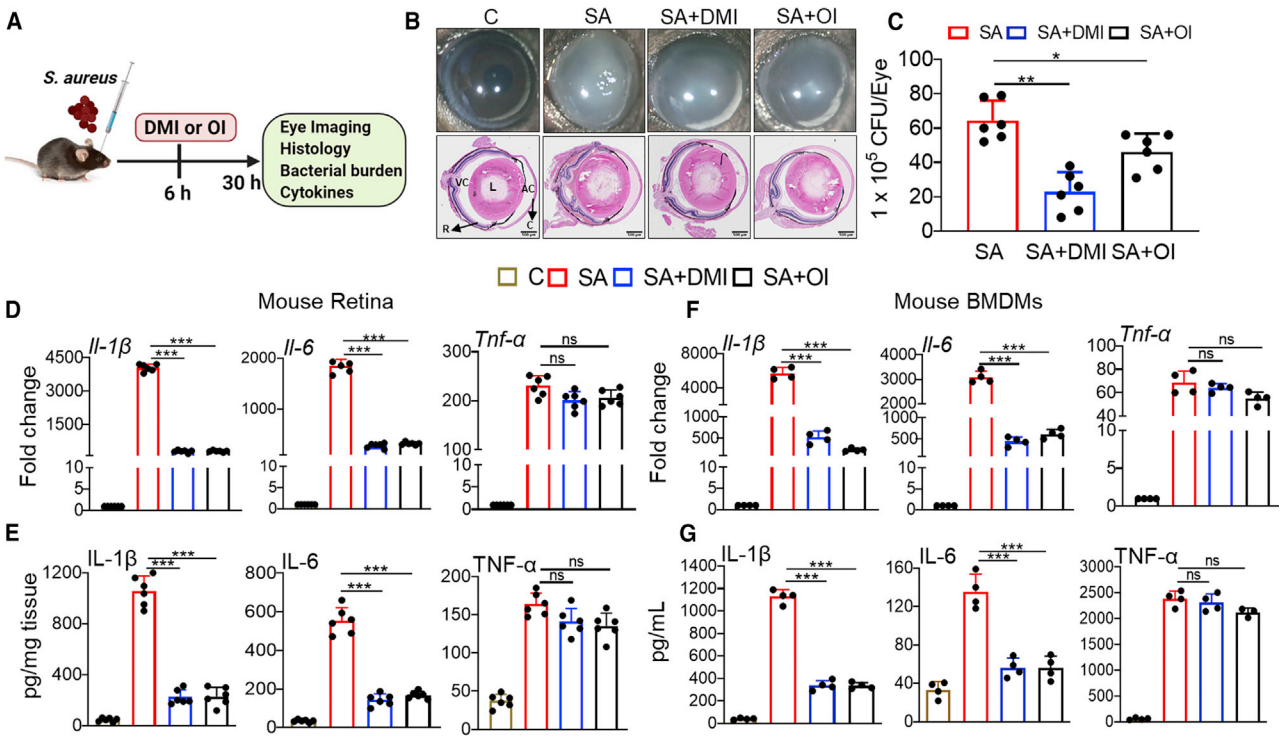

Figure 4. The itaconate derivatives, DMI and OI, ameliorate bacterial endophthalmitis

(A–E) Endophthalmitis was induced in the eyes of B6 WT mice by intravitreal inoculation of *S. aureus* (SA) RN6390 (5000 CFUs/eye). After 6 h, eyes were treated with either DMI or OI (10 μg/eye) via intravitreal injection. (A) Schematic showing a timeline for induction of endophthalmitis, itaconate treatment, and assays used to monitor disease progression. (B, top panel) Representative slit-lamp micrograph showing corneal haze/opacity in eyes under the indicated conditions 24 h after itaconate treatment. (B, bottom panel) H&E staining of enucleated eyes (n = 6). (C) Quantitation of intraocular bacterial burden in whole-eye lysates by serial dilution and plate counting, which is represented as CFUs/eye (n = 6). (D) The inflammatory cytokines in the retinas of mice at the indicated groups (n = 6) were measured by qPCR and are represented as relative fold change by normalizing gene expression with that of endogenous β-actin. (E) Quantification of protein levels of inflammatory cytokines in whole-eye lysates as determined by ELISA (n = 6).

(F and G) BMDMs from B6 WT mice (n = 4) were pretreated with DMI or OI (125 μM) for 2 h, followed by infection with *S. aureus* (MOI 10:1) for 8 h. The inflammatory cytokines were measured by qPCR (F) and represented as relative fold change by normalizing gene expression with that of endogenous β-actin (G). Quantification of protein levels of the indicated inflammatory cytokines in conditioned media from BMDMs, as determined by ELISA (n = 4).

The data represented are the culmination of two to four independent experiments and are shown as means ± SD. Statistical analysis was performed using one-way ANOVA with Tukey's multiple comparison test by comparing *S.-aureus*-infected samples with or without DMI/OI treatment. ns; non-significant, *$p < 0.05$, **$p < 0.001$, ***$p < 0.0001$. C, cornea; AC, anterior chamber; L, lens; VC, vitreous chamber; R, retina. See also Figure S3.

Itaconate treatment ameliorates bacterial endophthalmitis

The elevated levels of itaconate observed in the vitreous of patients with bacterial endophthalmitis, who are unlikely to have a deficiency of IRG1, suggest itaconate may harbor protective properties. To test that possibility, we used a non-resolving infection model (i.e., a higher infective dose of 5,000 CFUs/eye) to mimic the severe bacterial endophthalmitis that leads to blindness in humans and tested the therapeutic efficacy of two itaconate derivatives, dimethyl itaconate (DMI) and OI. Mice were treated with a single intravitreal injection of DMI or OI 6 h after infection with a high dose of *S. aureus* (Figure 4A). Disease progression was evaluated 24 h after itaconate treatment by performing ophthalmic exams (slit-lamp microscopy) and histopathological analysis, assessing retinal function, and estimating intraocular bacterial burden and inflammation. In mice infected with *S. aureus,* DMI or OI treatments markedly reduced the corneal haze/opacity and hypopyon as compared with those without treatment (Figure 4B, top panel). Histopathological analyses showed a striking reduction in retinal tissue damage and cellular infiltration in mice treated with the itaconate derivatives (Figure 4B, bottom panel). Additionally, both DMI and OI treatment significantly reduced bacterial burden in the eyes of infected mice, with DMI treatment having a greater anti-bacterial effect (Figure 4C).

In addition to direct retinal damage as a result of bacterial toxins,[29] the pathogenesis of bacterial endophthalmitis leads to ocular injury from excessive activation of inflammatory pathways.[33] Thus, we assessed intraocular inflammation and found that itaconate treatment (either DMI or OI) drastically reduced expression of the inflammatory cytokines IL-1β and IL-6 at the gene (Figure 4D) and protein (Figure 4E) levels. Surprisingly, the levels of TNF-α remained unchanged, irrespective of treatment, indicating differential effects of itaconate on inflammatory molecules. Similar to our *in vivo* observation, DMI/OI treatment significantly reduced inflammatory cytokines (IL-1β and IL-6) at

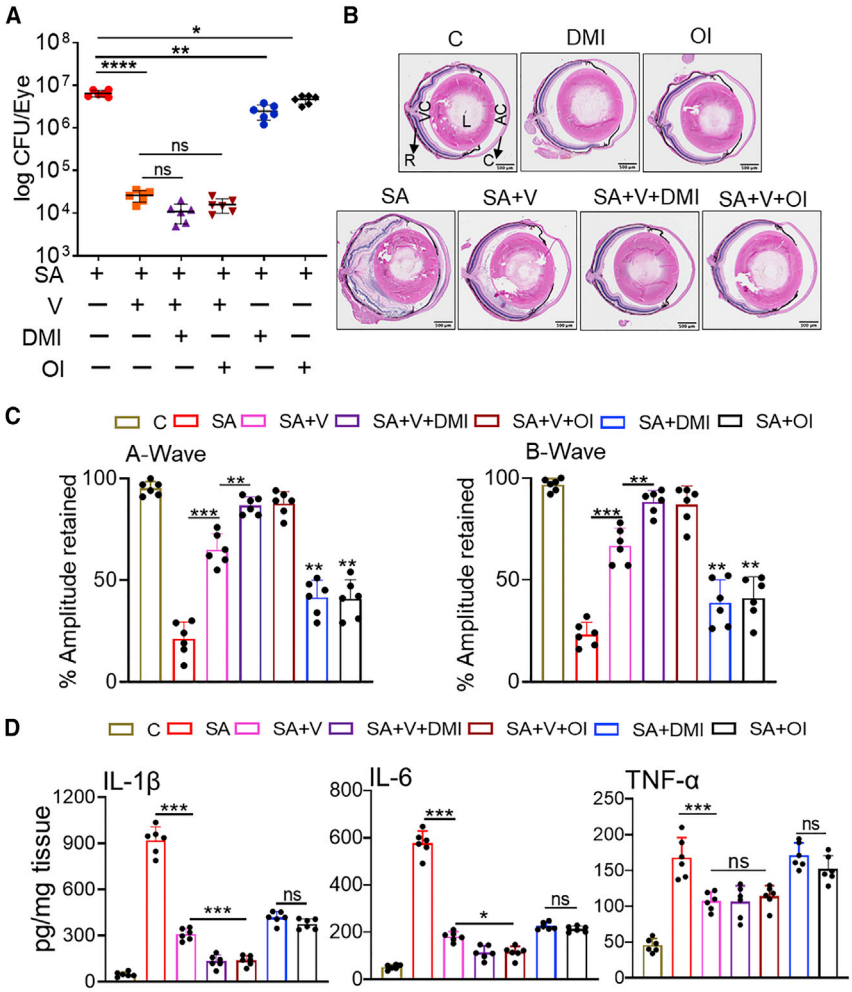

Figure 5. Itaconate synergizes with antibiotics to attenuate intraocular inflammation in bacterial endophthalmitis

Endophthalmitis was induced in the eyes of WT mice (n = 6/group). Six hours after infection, eyes were treated by intravitreal injection with vancomycin (V, 0.6 μg/eye) or DMI or OI (10 μg/eye) either alone or in the indicated combinations. Twenty-four hours after drug treatment, eyes were enucleated for analysis.

(A) Bacterial burden was estimated by serial dilution and plate count method.

(B) Representative H&E staining of enucleated eyes treated as indicated. C, cornea; AC, anterior chamber; L, lens; VC, vitreous chamber; R, retina.

(C) Percentage of a- and b-wave amplitudes retained in scotopic ERG recorded from WT mice eyes after *S. aureus* (SA) infection and itaconate/vancomycin treatment.

(D) Quantification of the indicated inflammatory cytokines in whole-eye lysates as determined by ELISA.

The data represented are the culmination of two to three independent experiments and are shown as means ± SD. Statistical analysis was performed using one-way ANOVA with Tukey's multiple comparison test by comparing *S. aureus*-infected samples with or without treatment. ns; non-significant, *p < 0.05, **p < 0.001, ***p < 0.0001. See also Figure S4.

the level of the transcript (Figure 4F) and protein (Figure 4G) in WT BMDMs. In addition, DMI/OI treatment reduced the generation of reactive oxygen species (ROS) in *S. aureus*-infected BMDMs (Figure S3A), indicating its ability to diminish oxidative stress.[34] Collectively, these results indicate that itaconate exerts both antibacterial and anti-inflammatory properties during bacterial endophthalmitis.

As in similar studies, we used the cell-permeable derivatives of itaconate and demonstrated their anti-inflammatory role in the eye. However, some recent reports show that the itaconate derivatives (DMI and OI), exert different mechanisms compared with endogenous itaconate in regulating inflammation.[35,36] Thus, we tested the effect of pH-buffered (pH 7.0) itaconic acid (ITA), along with OI, in our disease model. We found that ITA treatment also reduced corneal haze/opacity and hypopyon (Figure S3B) and bacterial burden (Figure S3C) in *S. aureus*-infected eyes. Similarly, ITA was found to attenuate the expression of the inflammatory cytokines at transcript (Figure S3D) and protein (Figure S3E) levels. However, the comparative analysis revealed that OI was superior to ITA in reducing intraocular inflammation, supporting its use to treat ocular infections.

Itaconate synergizes with antibiotics to reduce inflammation and disease severity

Intravitreal injection of antibiotics (vancomycin and ceftazidime) is currently the only standard treatment for managing bacterial endophthalmitis.[37] However, emerging resistance to antibiotics among common ocular pathogens necessitates an increased and continuous evaluation of the best antibiotic treatment for this condition.[38] The anti-inflammatory effects of itaconate suggest that it could be used as an adjunct therapeutic in combination with antibiotics to ameliorate bacterial endophthalmitis. To test that, we first determined the minimum inhibitory concentrations (MICs) of vancomycin (V), DMI, and OI against *S. aureus* strain RN6390 (Figure S4), which were found to be 2.5 μg/mL, 10 mg/mL, and 12.5 mg/mL, respectively. Next, sub-MIC levels of vancomycin were used either alone or in a combination with DMI or OI (e.g., V+DMI or V+OI) to treat *S. aureus*-infected eyes. As expected, treatment with vancomycin drastically reduced bacterial burden, yet the combined treatment of both V+DMI or V+OI further reduced viable bacterial counts (Figure 5A). Moreover, the combination therapy protected the retina from tissue damage (Figure 5B) and preserved retinal function with better retention of a- and b-wave amplitudes relative to treatment with V, DMI, or OI alone (Figure 5C). Similarly, the levels of inflammatory mediators were significantly diminished in eyes treated with combination therapy as compared with V, DMI, and OI treatments alone (Figure 5D). These results suggest the potential use of itaconate as

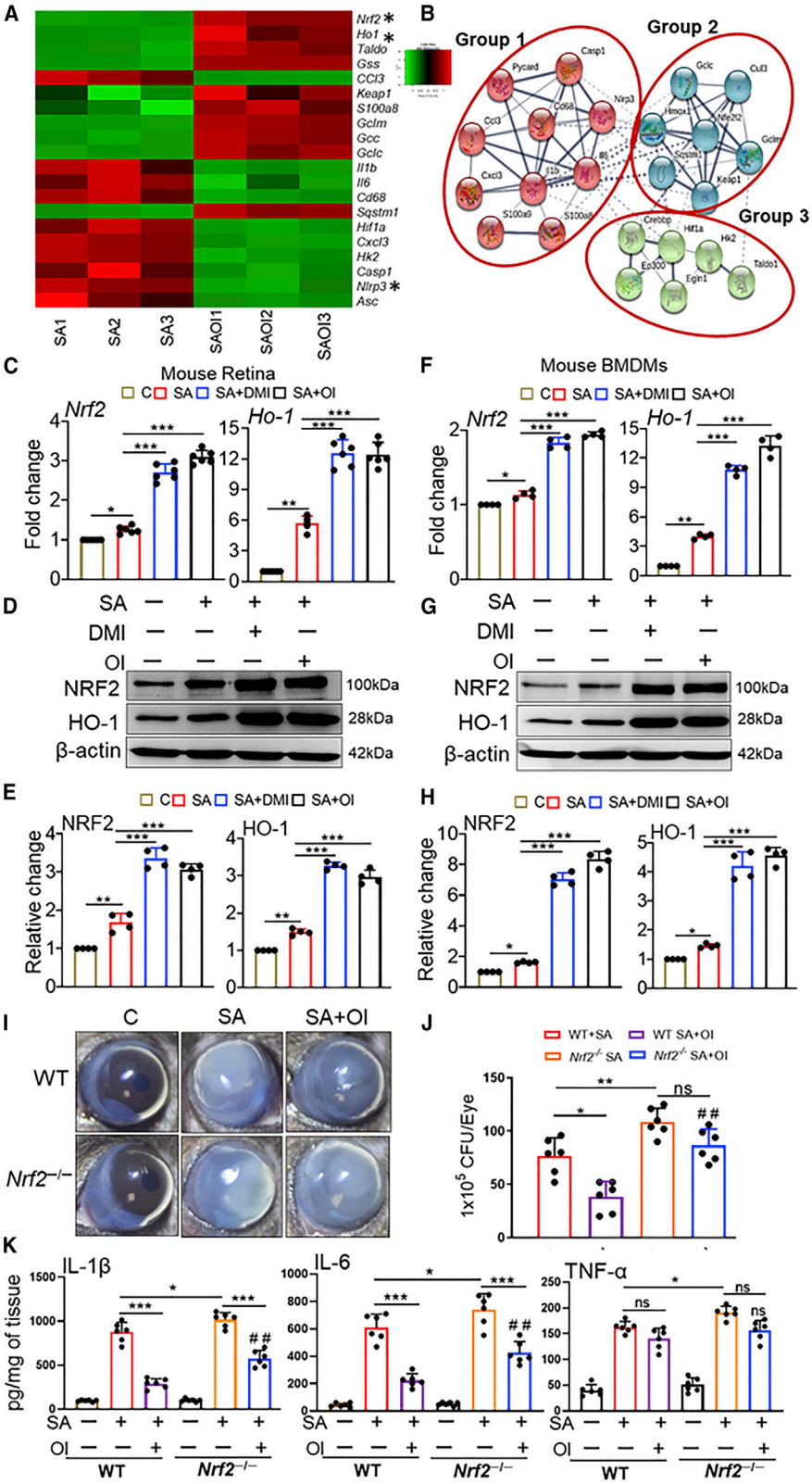

(legend on next page)

an adjunct therapy to complement the antibiotic treatment of bacterial endophthalmitis and potentially lower the antibiotic dosage required for the treatment of this condition.

Itaconate exerts its anti-inflammatory effect by potentiating NRF2/HO-1 signaling

To understand the protective mechanisms evoked by itaconate, we performed RNA sequencing (RNA-seq) analysis of WT BMDMs infected with *S. aureus* in the presence or absence of OI. Itaconate modulated the expression of a total 355 genes (212↑; and 143↓), including those which regulate antioxidant (e.g., *Nrf2* and *Ho-1*), innate immunity, immune activation, and inflammasome pathways (Figure 6A). We analyzed the top 20 DEGs based on the proteins they encode to generate a protein-protein interaction map (Figure 6B). This revealed that itaconate may affect genes encoding proteins associated with the inflammasome (group 1) and that are involved in antioxidant pathways (group 2). Prior studies have shown that itaconate exerts its anti-inflammatory effects via *Nrf2*,[39] which, along with its downstream target gene *Ho-1*, was differentially expressed in our analysis. Therefore, we set out to determine the role of *Nrf2* and *Ho-1* in our disease model (Figure S5A).

We found *S. aureus* infection induced the expression of *Nrf2* and *Ho-1* in mouse retina and DMI or OI treatment potentiated their expression both at the transcript (Figure 6C) and protein (Figures 6D and 6E) levels. The induction and potentiation of *Nrf2* and *Ho-1* at the transcript (Figure 6F) and protein (Figures 6G and 6H) levels was also observed in *S. aureus*-infected and OI-treated WT BMDMs. Like DMI/OI, itaconic acid (ITA) also induced the expression of *Nrf2* and *Ho-1* in *S. aureus*-infected mouse retina (Figure S5B), albeit at lower levels than OI induced, suggesting the involvement of *Nrf2* in both endogenous and exogenously administered itaconate derivatives in the eye. We also assessed *Nrf2*/*Ho-1* signaling in BMDMs from *Irg1*$^{-/-}$ mice and found no significant induction of *Nrf2* and *Ho-1* transcripts (Figure S5C) or protein (Figure S5D), in response to *S. aureus* infection alone. However, DMI/OI treatment markedly induced NRF2 and HO-1 expression. These results indicate that *Irg1* deficiency (i.e., reduced endogenous itaconate) impaired NRF2/HO-1 antioxidant pathway in ocular infections.

We also assessed the effect of DMI and OI on *Nrf2* and *Ho-1* expression in the human retinal Müller glia cell line MIO-M1. Cells that were infected with *S. aureus* and treated with either DMI or OI showed increased expression of *Nrf2* and *Ho-1* at both the mRNA (data not shown) and protein levels (Figures S5E and S5F). Because DMI and OI were found to synergize with vancomycin in reducing intraocular inflammation (Figure 5), we determined whether the combination therapy also boosted antioxidant pathways. Our data show that *in vivo*, the combination of vancomycin and DMI or OI significantly increased expression of *Nrf2* and *Ho-1* transcripts as compared with vancomycin or itaconate alone (Figures S5G and S5H).

The ability of itaconate to induce NRF2 and HO-1 expression in both *in vivo* and *in vitro* models suggests that NRF2/HO-1 signaling regulates the inflammatory response in bacterial endophthalmitis. Therefore, to test that hypothesis, we used small hairpin RNAs (shRNAs) to silence their expression in WT BMDMs. Knockdown of NRF2 and HO-1 at the protein level was confirmed by western blot (Figure S6A) and that led to increased expression of *S. aureus*-induced inflammatory mediators (Figure S6B). To further validate the anti-inflammatory role of NRF2 signaling in our model, we used *Nrf2*$^{-/-}$ mice. As expected, OI treatment significantly reduced corneal haze, opacity, and hypopyon in WT mice; however, that effect was diminished in *Nrf2*$^{-/-}$ mice (Figure 6I). A similar trend of relatively lower antibacterial (Figure 6J) and anti-inflammatory (Figure 6K) properties of OI was observed in *Nrf2*$^{-/-}$ versus WT mice. ERG analysis also revealed that, although OI treatment significantly retained retinal function (i.e., amplitudes of a- and b-waves) in both WT and *Nrf2*$^{-/-}$ mice compared with the untreated eye, the percentage retention was more in the WT mice. (Figure S6C). *In vitro* studies showed significant induction of NRF2 and HO-1 in DMI or OI treated WT BMDMs but not in *Nrf2*$^{-/-}$ BMDMs (Figure S6D). Like *in vivo* observation, reduced anti-inflammatory effects of OI and DMI were observed in *Nrf2*$^{-/-}$ BMDMs compared with WT cells (Figure S6E). Collectively, these results indicate that OI/DMI treatment was more effective in protecting WT as compared with *Nrf2*$^{-/-}$ mouse eyes, indicating the role of NRF2/HO-1 signaling in regulating ocular inflammation in bacterial endophthalmitis.

Figure 6. Itaconate potentiates NRF2/HO-1 signaling in *S. aureus*-infected mouse retina and BMDMs

(A and B) BMDMs from WT mice (n = 3/condition) were either left untreated or pre-treated with OI (125 μM) for 2 h, followed by infection with *S. aureus* for 8 h. RNA was extracted, and RNA sequencing was performed using the Illumina platform. (A) Heatmap showing DEGs in *S. aureus* (SA)-infected and OI-treated BMDMs. (B) The DEGs shown in (A) were analyzed using the String database (version 11.0) to create a protein-protein interaction network. Group-1: genes involved in the inflammasome pathway. Group-2: genes involved in the antioxidant pathway. Group-3: transcription factors and hypoxia-inducible factor. Thick lines denote strong evidence of interactions, and dotted lines represent possible interactions among the genes in these pathways.

(C–E) After induction of *S. aureus* (SA) endophthalmitis and itaconate (DMI or OI) treatment, mouse retinas (n = 6) were used to quantitate *Nrf2* and *Ho-1* transcripts by qPCR (C) and protein expression by western blot with densitometry (n = 4) (D and E), normalized with β-actin and HSP90 as endogenous controls, respectively.

(F–H) BMDMs from WT mice were pretreated with DMI or OI (125 μM) for 2 h, followed by infection with *S. aureus* (MOI 10:1) for 8 h (n = 4). *Nrf2* and *Ho-1* expression was assessed by qPCR (F) and western blot with densitometry (n = 4) (G and H), normalized with β-actin and HSP90 as endogenous controls, respectively.

(I–K) Endophthalmitis was induced in the eyes of WT and *Nrf2*$^{-/-}$ mice (n = 6). After 6 h, eyes were treated with OI (10 μg/eye) via intravitreal injection. (I) Representative slit-lamp micrograph showing corneal haze/opacity at 24 h after itaconate treatment. (J) Quantitation of intraocular bacterial burden in whole-eye lysates by serial dilution and plate counting method. (K) The inflammatory cytokines in whole-eye lysates were determined by ELISA (n = 6).

The data represented are the culmination of two to four independent experiments and are shown as means ± SD. Statistical analysis was performed using one-way (C, E, F, and H) or two-way (J and K) ANOVA with Tukey's multiple comparison test by comparing *S. aureus*-infected samples with or without OI treatment. (# indicates comparison between WT versus *Nrf2*$^{-/-}$; J and K). ns; non-significant, *p < 0.05, # #**p < 0.001, ***p < 0.0001. See also Figures S5 and S6.

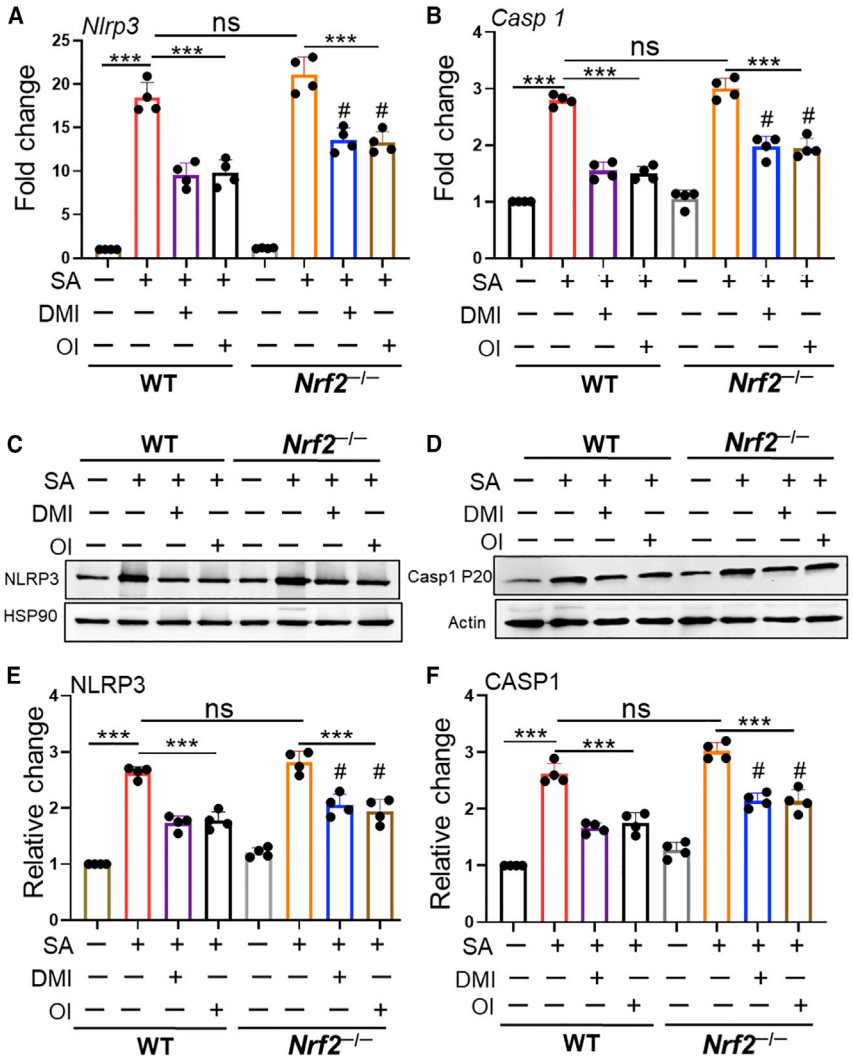

Figure 7. Itaconate inhibits *S. aureus*-induced activation of the NLRP3 inflammasome

(A and B) BMDMs from WT and *Nrf2*$^{-/-}$ mice (n = 4/condition) either were left untreated or were pretreated with DMI or OI (125 μM) for 2 h, followed by infection with *S. aureus* (SA) (MOI 10:1) for 8 h. *Nlrp3* (A) and *Casp1* (B) expression were assessed by qPCR. The data are expressed as relative fold change by normalizing gene expression to that of the endogenous β-actin gene.

(C and D) Western blot detection of NLRP3 (C) and cleaved caspase-1 (D) proteins.

(E and F) Densitometry analysis was performed using ImageJ, and data are expressed as relative fold changes normalized to the loading control, HSP90.

The data represented are the culmination of two to four independent experiments and are shown as means ± SD. Statistical analysis was performed using one-way ANOVA with Tukey's multiple comparison test by comparing *S. aureus*-infected samples with or without DMI or OI treatment. (# indicates comparison between WT versus *Nrf2*$^{-/-}$; A, B, E, and F). ns; non-significant, $^{\#}p < 0.05$, $^{**}p < 0.001$, $^{***}p < 0.0001$.

Itaconate inhibits the expression of bacterial-induced NLRP3 and Caspase−1

Thus far, our studies showed that *S. aureus* induces the production of IL-1β in both the mouse retina and in cultured BMDMs and that itaconate attenuated that response. Because activation of the NLRP3 inflammasome is primarily responsible for the cleavage of pro-IL-1β into active IL-1β via activation of caspase 1, we sought to determine the effect of itaconate on NLRP3 activation. Using WT and *Nrf2*$^{-/-}$ BMDMs, our data showed that *S. aureus* induced the expression of *Nlrp3* (Figure 7A) and caspase-1 (Figure 7B) transcripts, whereas DMI or OI treatment significantly inhibited their expression in both cell types, albeit more in WT BMDMs. This observation was confirmed by western blot for NLRP3 (Figures 7C and 7E) and cleaved caspase 1 P20 (Figures 7D and 7F), which showed inhibition of NLRP3 and Casp-1 in DMI- or OI-treated WT BMDMs. These findings indicate that itaconate attenuates the NLRP3-Casp-1-IL-1β cascade to downregulate ocular inflammation, and *Nrf2* is partially involved in that phenomenon.

DISCUSSION

The incidence of bacterial endophthalmitis is on the rise, and current treatments are often inadequate in preventing adverse outcomes, necessitating the discovery of alternative therapeutics that alleviate the underlying pathophysiology of this condition. However, the immune-privilege status of the eye poses significant challenges in treating ocular infections. Ophthalmologists have generally been reluctant to prescribe adjunctive anti-inflammatory drugs, such as corticosteroids, because of their immunosuppressive effects.[40–42] Thus, there is significant interest in identifying biologic agents and immunomodulatory therapies that target ocular inflammation without major disruption to the normal immune response in the eye.[33,43]

Here, we used an integrated transcriptomic[10] and untargeted metabolomics[11] approach to identify genes and metabolites involved in experimental bacterial endophthalmitis. Using the vitreous of human patients and mouse eyes during bacterial endophthalmitis, we identified an increase in the expression of *Irg1* and the concentration of its metabolite, itaconate, and that there was a strong pairwise correlation between the two upon infection with *S. aureus*. Given the anti-inflammatory role of itaconate,[44] we hypothesized that activation of the *Irg1*/itaconate axis promotes resolution of inflammation during bacterial endophthalmitis. Using *Irg1*$^{-/-}$ mice and through shRNA-mediated gene silencing, we demonstrate that itaconate exerts protective effects by modulating NRF2/HO1 signaling. Most notably, intraocular administration of itaconate either alone or in combination with antibiotic treatment drastically improved disease outcomes.

Collectively, our study reveals an essential role of IRG1 and itaconate in regulating protective responses during bacterial infection in the eye and suggests a model wherein intraocular administration of itaconate reduces inflammation and bacterial burden to ameliorate bacterial endophthalmitis. Thus, our study demonstrates considerable promise for the translation of an itaconate-based treatment strategy to mitigate ocular bacterial infections.

An increasing number of studies have shown that under inflammatory stimuli (e.g., LPS challenge), *Irg1* is expressed, and consequently, itaconate is produced in macrophages.[23,45,46] However, the role of *Irg1*/itaconate remains largely unknown in the pathobiology of eye diseases, especially in ocular bacterial infections. Here, we show that *Irg1* is upregulated both *in vivo* (mouse retina) and *in vitro* (BMDMs and human retinal Müller glia) during *S. aureus* infection. Moreover, induced *Irg1* expression coincided with an increased accumulation of itaconate in infected mouse eyes, which was also consistent with elevated levels observed in the vitreous of patients with culture-positive bacterial (both Gram-positive and Gram-negative) endophthalmitis. The increased itaconate levels in Gram-negative infection are likely due to LPS, which is known to induce *Irg1* and is abundantly present in Gram-negative bacterial cell walls.[47,48] Here, we show that among the *S. aureus* virulence factors, cell-wall components, but not the toxins, are the inducers of *Irg1* expression, which is consistent with our prior study showing their inflammatory role in the eye.[29,49] Together, these findings provide the evidence for the involvement of the *Irg1*/itaconate pathway in ocular infection.

In the absence of *Irg1,* we found mice are more susceptible to developing bacterial endophthalmitis, even when subjected to a lower infectious dose of bacteria that is usually resolved in WT mice. *Irg1*$^{-/-}$ mice had a higher bacterial burden, increased inflammatory mediators, and more tissue damage, culminating in the loss of retinal/visual function. This is in agreement with other studies showing increased infection and inflammation in *Irg1*$^{-/-}$ mice in response to *Mtb*, leading to greater mortality rates.[50] As anticipated, BMDMs from *Irg1*$^{-/-}$ mice had reduced itaconate levels, and supplementing those mice with itaconate derivatives ameliorated bacterial endophthalmitis by reducing intraocular inflammation and preserving retinal tissue, suggesting itaconate could serve as a therapeutic option for humans with this condition. However, humans with this condition are likely not commonly deficient for IRG1. Therefore, we assessed the therapeutic efficacy of itaconate in WT mice with *S. aureus* endophthalmitis and observed profound protection. This suggests interventions that enhance *Irg1* expression and/or itaconate levels within the eye could present potential therapeutic strategies for the treatment of ocular bacterial infections.

The clinical outcomes of bacterial endophthalmitis depend upon both the virulence of the infecting organism and the time at which appropriate therapy is initiated. Because of the poor penetration of systemic antibiotics, intravitreal injections of antibiotics remain the most widely accepted treatment option to manage the condition.[51] Although these intraocular antibiotics eliminate the bacterial infection, they often liberate bacterial cell wall components,[52,53] contributing to bystander inflammatory damage to ocular tissue.[29] Given the anti-inflammatory and antimicrobial role of itaconate[24,46,54] and its elevated levels in patients with endophthalmitis, we tested its therapeutic potential when co-administered with antibiotics. Notably, co-administration of itaconate with sub-MIC concentrations of vancomycin significantly reduced ocular inflammation and improved disease outcomes. Thus, our study provides evidence that the combination of antibiotics and itaconate function synergistically to ameliorate endophthalmitis and reduce ocular inflammation. Moreover, including itaconate as an anti-inflammatory therapy could reduce the overall dosage of antibiotics required to treat bacterial endophthalmitis.

Macrophages[13] and Müller glia[34,55] are known to have essential roles in orchestrating retinal innate responses in bacterial endophthalmitis, and our RNA-seq analysis in *S. aureus*-infected BMDMs indicated that NRF2/HO-1 and NLRP3 signaling are differentially modulated by itaconate treatment. Both itaconate derivatives, DMI and OI, potentiated the expression of NRF2 and its downstream signaling molecule HO1 in *S. aureus*-infected BMDMs and human retinal Müller glia. Moreover, levels of NRF2 and HO1 were increased in the mouse retina treated with itaconate. The reduction in inflammatory mediators upon itaconate treatment in *S. aureus*-infected cultured cells and its reversal by silencing *Nrf2* indicate that itaconate likely exerts its anti-inflammatory effects in the eye by regulating NRF2/HO1 signaling. The mechanisms for anti-inflammatory effects of itaconate have been reported to involve the inhibition of succinate dehydrogenase,[26,56] blockade of IκBζ translation,[57] and activation of NRF2.[39] Although our data support the idea of itaconate-induced *Nrf2*/*Ho-1* antioxidant signaling in exerting protective effects,[39,58,59] recent studies report distinct mechanisms for endogenous itaconate versus its derivatives in regulating inflammation.[35,36] The itaconate derivative OI reduces inflammation by triggering electrophilic stress, which is compensated by activation of the antioxidant *Nrf2*/*Ho-1* axis, whereas endogenous itaconate evokes NRF2-independent mechanisms.[35] However, a more recent study using $^{13}C_5$-labeled OI showed that exogenously added OI can directly generate endogenous itaconate and reduce inflammation by carboxypropylation of NLRP3 and prohibiting its interaction with NEK7, which is essential for inflammasome activation.[60] Therefore, those authors argued that OI could be used as a surrogate to study itaconate because it can be taken up and converted to intracellular itaconate by macrophages. We also found that OI treatment reduced NLRP3 coinciding with attenuated IL-1β secretion.

In view of recent studies and to clarify whether DMI- or OI-mediated protection is dependent on *Nrf2* signaling, we used *Nrf2*$^{-/-}$ mice. Our data showed that (1) in comparison to WT mice, infected *Nrf2*$^{-/-}$ mouse eyes had higher inflammation and bacterial burden; and (2) the protective and anti-inflammatory effects of OI were reduced but not completely abolished in *Nrf2*$^{-/-}$ mice. Previous studies investigating the *Irg1*/itaconate axis have used LPS-stimulated macrophages. In contrast, we used live bacteria (which possess multiple virulence factors), and the observed differences in *Nrf2* dependency could be attributed to the nature of the inflammatory stimuli. Nonetheless, we conclude that *Nrf2* signaling, in part, contributes to OI-mediated protection, and *Nrf2* deficiency exacerbates *S. aureus* endophthalmitis. Our data show that *S. aureus* induced NLRP3/Casp1 expression and IL-1β secretion in WT BMDMs, and *Nrf2*

silencing or knockout (*Nrf2*$^{-/-}$) potentiated IL-1β levels. However, in *Nrf2*$^{-/-}$ BMDMs, although, reduced by OI or DMI treatments, NLRP3/Casp1 levels did not change by *S. aureus* alone, indicating *Nrf2*-independent regulation of NLRP3 inflammasome. Some potential mechanisms by which *S. aureus* could activate NLRP3/Casp-1 in an *Nrf2*-independent manner include (1) induction of oxidative (i.e., ROS generation; Figure S3A) and endoplasmic reticulum (ER) stress,[61] which can directly activate NLRP3/Casp1/IL-1β cascade;[62,63] and (2) the production of saturated fatty acids, such as palmitate, under inflammatory conditions in the retina,[64,65] which could also trigger NLRP3 activation, leading to IL-1β and IL-18 production.[66] We acknowledge that further studies using *Irg1* and *Nrf2; Nlrp3* and *Nrf2* double knockout mice and cells are needed to determine the role of endogenous itaconate and to dissect *Irg1-Nrf2-Nlrp3* crosstalk in ocular infection.

Controlling intraocular inflammation is an effective approach to improve the outcome of ocular infections. In support of that, our results provide evidence of the effectiveness of itaconate as adjunctive therapy with antibiotics to treat bacterial endophthalmitis by reducing the bacterial burden and correcting the dysregulated inflammatory response, thus preventing ocular tissue damage.

Limitations of study

Despite the importance of these findings, there are a few limitations to our study that should be considered. First, elevated levels of itaconate were detected in both Gram-positive and Gram-negative bacterial endophthalmitis, whereas we only tested the effect of itaconate in a *S. aureus* (e.g., Gram-positive) infection model. In a recent study, itaconate was found to exacerbate *Pseudomonas* lung infection.[67] Therefore, additional studies are needed to evaluate the effect of itaconate in Gram-negative ocular infections. Second, we only evaluated the therapeutic efficacy of itaconate at 6 h after infection. However, patients may not seek treatment until they experience pain and blurry vision, indicative of an advanced disease state. Hence, the timing (e.g., too early or very late) of treatment and optimal dose of anti-inflammatory therapy must be further studied because excessive suppression of inflammation could reduce the ability of the host to mount a sufficient antimicrobial response. Corresponding with that, the efficacy of itaconate as an adjunct therapeutic needs to be compared with ocular corticosteroids and evaluated with other types of antibiotics used to treat ocular infections. Although we observed reduced inflammation and protection in itaconic-acid-treated eyes, the effect was not as profound as that of OI. As reported recently, alteration of the itaconate structure in DMI or OI is responsible for extra effects that may not be attributed to itaconate.[35] Therefore, itaconate derivatives used in this study may not fully recapitulate the endogenous itaconate mode of action and warrant further investigation. We also acknowledge that the amount of itaconate (4OI [~41 mM] and DMI [~63 mM]) administered was greater than the endogenous itaconate levels (~55–120 pM at 24 h after infection) detected in the mouse eyes. Additional time kinetics studies are needed to determine the physiological range of itaconate in both human and mouse eyes.

STAR★METHODS

Detailed methods are provided in the online version of this paper and include the following:

- KEY RESOURCES TABLE
- RESOURCE AVAILABILITY
  - Lead contact
  - Materials availability
  - Data and code availability
- EXPERIMENTAL MODEL AND SUBJECT DETAILS
  - Mice and ethics statement
  - Mouse model of bacterial endophthalmitis
  - Patient vitreous collection
  - Cell and culture conditions
- METHOD DETAILS
  - Bacterial burden estimation
  - Isolation of bone marrow-derived macrophages
  - Determination of the minimum inhibitory concentration (MIC)
  - RNA extraction and real-time PCR
  - Histology
  - Cytokine ELISA
  - Measurement of intracellular reactive oxygen species (ROS)
  - shRNA mediated knockdown
  - Western blotting
  - Liquid chromatography coupled with a tandem mass spectrometer (LC-MS/MS)
  - Preprocessing and annotation of metabolomic and transcriptomic data
  - Metabolomic and transcriptomic data analysis
- QUANTIFICATION AND STATISTICAL ANALYSIS

SUPPLEMENTAL INFORMATION

Supplemental information can be found online at https://doi.org/10.1016/j.xcrm.2021.100277.

ACKNOWLEDGMENTS

This study is supported by the National Institutes of Health grants R01EY026964, R01EY027381, and R21AI140033 (A.K.) and an unrestricted grant to the Department of Ophthalmology, Visual, and Anatomical Sciences from Research to Prevent Blindness (RPB). The immunology resource core is supported by NIH center grant P30EY004068. S.G. is supported by National Institutes of Health grants NS112727 and AI144004. The funders had no role in study design, data collection, and interpretation, or the decision to submit the work for publication. The authors are grateful to Prof. Luke A. O'Neill, Trinity College Dublin, Ireland, for his kind gift for 4-octyl itaconate. We are thankful for the pharmacology and metabolomics core, Karmanos Cancer Institute, Wayne State University, for the estimation of itaconate. The authors are also thankful to Robert Wright for the technical support and other members of the laboratory for their helpful discussion and editing of the final manuscript.

AUTHOR CONTRIBUTIONS

A.K. conceived the idea and designed experiments and provided direction and funding for the project. S.S. and P.K.S. designed and performed the experiments, analyzed the data, and prepared the figures. A.J. analyzed metabolomics and transcriptomic data. P.N. and J.J. collected human vitreous samples and performed itaconate measurements in those samples. S.S., P.K.S., and

A.K. wrote the manuscript. S.G. helped in experimental design, provided intellectual inputs, and critically reviewed the manuscript. All authors contributed to the editing of the final manuscript.

DECLARATION OF INTERESTS

The authors declare no competing interests.

Received: August 18, 2020
Revised: December 13, 2020
Accepted: April 19, 2021
Published: May 18, 2021

REFERENCES

1. Wu, A.M., Wu, C.M., Tseng, V.L., Greenberg, P.B., Giaconi, J.A., Yu, F., Lum, F., and Coleman, A.L. (2018). Characteristics associated with receiving cataract surgery in the US Medicare and Veterans Health Administration populations. JAMA Ophthalmol. *136*, 738–745.
2. Flaxman, S.R., Bourne, R.R.A., Resnikoff, S., Ackland, P., Braithwaite, T., Cicinelli, M.V., Das, A., Jonas, J.B., Keeffe, J., Kempen, J.H., et al.; Vision Loss Expert Group of the Global Burden of Disease Study (2017). Global causes of blindness and distance vision impairment 1990–2020: a systematic review and meta-analysis. Lancet Glob. Health *5*, e1221–e1234.
3. Astley, R.A., Coburn, P.S., Parkunan, S.M., and Callegan, M.C. (2016). Modeling intraocular bacterial infections. Prog. Retin. Eye Res. *54*, 30–48.
4. Naik, P., Singh, S., Dave, V.P., Ali, M.H., Kumar, A., and Joseph, J. (2020). Vitreous D-lactate levels as a biomarker in the diagnosis of presumed infectious culture negative endophthalmitis. Curr. Eye Res. *45*, 184–189.
5. Patel, S.N., Gangaputra, S., Sternberg, P., Jr., and Kim, S.J. (2020). Prophylaxis measures for postinjection endophthalmitis. Surv. Ophthalmol. *65*, 408–420.
6. Shivaramaiah, H.S., Relhan, N., Pathengay, A., Mohan, N., and Flynn, H.W., Jr. (2018). Endophthalmitis caused by gram-positive bacteria resistant to vancomycin: clinical settings, causative organisms, antimicrobial susceptibilities, and treatment outcomes. Am. J. Ophthalmol. Case Rep. *10*, 211–214.
7. Hanscom, T. (1996). The endophthalmitis vitrectomy study. Arch. Ophthalmol. *114*, 1029–1030, author reply 1028–1029.
8. Sadaka, A., Durand, M.L., and Gilmore, M.S. (2012). Bacterial endophthalmitis in the age of outpatient intravitreal therapies and cataract surgeries: host-microbe interactions in intraocular infection. Prog. Retin. Eye Res. *31*, 316–331.
9. Chu, H., Chan, J.F., Yuen, T.T., Shuai, H., Yuan, S., Wang, Y., Hu, B., Yip, C.C., Tsang, J.O., Huang, X., et al. (2020). Comparative tropism, replication kinetics, and cell damage profiling of SARS-CoV-2 and SARS-CoV with implications for clinical manifestations, transmissibility, and laboratory studies of COVID-19: an observational study. Lancet Microbe *1*, e14–e23.
10. Rajamani, D., Singh, P.K., Rottmann, B.G., Singh, N., Bhasin, M.K., and Kumar, A. (2016). Temporal retinal transcriptome and systems biology analysis identifies key pathways and hub genes in *Staphylococcus aureus* endophthalmitis. Sci. Rep. *6*, 21502.
11. Kumar, A., Singh, P.K., and Giri, S. (2016). Metabolic signatures of *Staphylococcus aureus* endophthalmitis. Invest. Ophthalmol. Vis. Sci. *57*, 5871.
12. Singh, P.K., Khatri, I., Jha, A., Pretto, C.D., Spindler, K.R., Arumugaswami, V., Giri, S., Kumar, A., and Bhasin, M.K. (2018). Determination of system level alterations in host transcriptome due to Zika virus (ZIKV) Infection in retinal pigment epithelium. Sci. Rep. *8*, 11209–11209.
13. Kumar, A., Giri, S., and Kumar, A. (2016). 5-Aminoimidazole-4-carboxamide ribonucleoside-mediated adenosine monophosphate-activated protein kinase activation induces protective innate responses in bacterial endophthalmitis. Cell. Microbiol. *18*, 1815–1830.
14. Francis, R., Singh, P.K., Singh, S., Giri, S., and Kumar, A. (2020). Glycolytic inhibitor 2-deoxyglucose suppresses inflammatory response in innate immune cells and experimental staphylococcal endophthalmitis. Exp. Eye Res., 108079.
15. Garcia, G., Jr., Paul, S., Beshara, S., Ramanujan, V.K., Ramaiah, A., Nielsen-Saines, K., Li, M.M.H., French, S.W., Morizono, K., Kumar, A., and Arumugaswami, V. (2020). Hippo signaling pathway has a critical role in Zika virus replication and in the pathogenesis of neuroinflammation. Am. J. Pathol. *190*, 844–861.
16. Kelly, B., and O'Neill, L.A.J. (2015). Metabolic reprogramming in macrophages and dendritic cells in innate immunity. Cell Res. *25*, 771–784.
17. Cordes, T., Wallace, M., Michelucci, A., Divakaruni, A.S., Sapcariu, S.C., Sousa, C., Koseki, H., Cabrales, P., Murphy, A.N., Hiller, K., et al. (2016). Immunoresponsive gene 1 and itaconate inhibit succinate dehydrogenase to modulate intracellular succinate levels. J. Biol. Chem. *291*, 14274–14284.
18. De Souza, D.P., Achuthan, A., Lee, M.K.S., Binger, K.J., Lee, M.-C., Davidson, S., Tull, D.L., McConville, M.J., Cook, A.D., Murphy, A.J., et al. (2019). Autocrine IFN-I inhibits isocitrate dehydrogenase in the TCA cycle of LPS-stimulated macrophages. J. Clin. Invest. *129*, 4239–4244.
19. Wang, H., Fedorov, A.A., Fedorov, E.V., Hunt, D.M., Rodgers, A., Douglas, H.L., Garza-Garcia, A., Bonanno, J.B., Almo, S.C., and de Carvalho, L.P.S. (2019). An essential bifunctional enzyme in Mycobacterium tuberculosis for itaconate dissimilation and leucine catabolism. Proc. Natl. Acad. Sci. USA *116*, 15907–15913.
20. Wang, P., Xu, J., Wang, Y., and Cao, X. (2017). An interferon-independent lncRNA promotes viral replication by modulating cellular metabolism. Science *358*, 1051–1055.
21. Nair, S., Huynh, J.P., Lampropoulou, V., Loginicheva, E., Esaulova, E., Gounder, A.P., Boon, A.C.M., Schwarzkopf, E.A., Bradstreet, T.R., Edelson, B.T., et al. (2018). *Irg1* expression in myeloid cells prevents immunopathology during *M. tuberculosis* infection. J. Exp. Med. *215*, 1035–1045.
22. Domínguez-Andrés, J., Novakovic, B., Li, Y., Scicluna, B.P., Gresnigt, M.S., Arts, R.J.W., Oosting, M., Moorlag, S.J.C.F.M., Groh, L.A., Zwaag, J., et al. (2019). The itaconate pathway is a central regulatory node linking innate immune tolerance and trained immunity. Cell Metab. *29*, 211–220.e5.
23. Michelucci, A., Cordes, T., Ghelfi, J., Pailot, A., Reiling, N., Goldmann, O., Binz, T., Wegner, A., Tallam, A., Rausell, A., et al. (2013). Immune-responsive gene 1 protein links metabolism to immunity by catalyzing itaconic acid production. Proc. Natl. Acad. Sci. USA *110*, 7820–7825.
24. Meiser, J., Kraemer, L., Jaeger, C., Madry, H., Link, A., Lepper, P.M., Hiller, K., and Schneider, J.G. (2018). Itaconic acid indicates cellular but not systemic immune system activation. Oncotarget *9*, 32098–32107.
25. Naujoks, J., Tabeling, C., Dill, B.D., Hoffmann, C., Brown, A.S., Kunze, M., Kempa, S., Peter, A., Mollenkopf, H.J., Dorhoi, A., et al. (2016). IFNs modify the proteome of *Legionella*-containing vacuoles and restrict infection via IRG1-derived itaconic acid. PLoS Pathog. *12*, e1005408.
26. Lampropoulou, V., Sergushichev, A., Bambouskova, M., Nair, S., Vincent, E.E., Loginicheva, E., Cervantes-Barragan, L., Ma, X., Huang, S.C., Griss, T., et al. (2016). Itaconate links inhibition of succinate dehydrogenase with macrophage metabolic remodeling and regulation of inflammation. Cell Metab. *24*, 158–166.
27. de Seymour, J.V., Conlon, C.A., Sulek, K., Villas Bôas, S.G., McCowan, L.M., Kenny, L.C., and Baker, P.N. (2014). Early pregnancy metabolite profiling discovers a potential biomarker for the subsequent development of gestational diabetes mellitus. Acta Diabetol. *51*, 887–890.
28. Weiss, J.M., Davies, L.C., Karwan, M., Ileva, L., Ozaki, M.K., Cheng, R.Y., Ridnour, L.A., Annunziata, C.M., Wink, D.A., and McVicar, D.W. (2018). Itaconic acid mediates crosstalk between macrophage metabolism and peritoneal tumors. J. Clin. Invest. *128*, 3794–3805.

29. Kumar, A., and Kumar, A. (2015). Role of *Staphylococcus aureus* virulence factors in inducing inflammation and vascular permeability in a mouse model of bacterial endophthalmitis. PLoS ONE *10*, e0128423.

30. Talreja, D., Singh, P.K., and Kumar, A. (2015). In vivo role of TLR2 and MyD88 signaling in eliciting innate immune responses in Staphylococcal endophthalmitis. Invest. Ophthalmol. Vis. Sci. *56*, 1719–1732.

31. Engelbert, M., and Gilmore, M.S. (2005). Fas ligand but not complement is critical for control of experimental *Staphylococcus aureus* endophthalmitis. Invest. Ophthalmol. Vis. Sci. *46*, 2479–2486.

32. Whiston, E.A., Sugi, N., Kamradt, M.C., Sack, C., Heimer, S.R., Engelbert, M., Wawrousek, E.F., Gilmore, M.S., Ksander, B.R., and Gregory, M.S. (2008). αB-crystallin protects retinal tissue during Staphylococcus aureus-induced endophthalmitis. Infect. Immun. *76*, 1781–1790.

33. Miller, F.C., Coburn, P.S., Huzzatul, M.M., LaGrow, A.L., Livingston, E., and Callegan, M.C. (2019). Targets of immunomodulation in bacterial endophthalmitis. Prog. Retin. Eye Res. *73*, 100763.

34. Singh, P.K., Shiha, M.J., and Kumar, A. (2014). Antibacterial responses of retinal Müller glia: production of antimicrobial peptides, oxidative burst and phagocytosis. J. Neuroinflammation *11*, 33.

35. Swain, A., Bambouskova, M., Kim, H., Andhey, P.S., Duncan, D., Auclair, K., Chubukov, V., Simons, D.M., Roddy, T.P., Stewart, K.M., and Artyomov, M.N. (2020). Comparative evaluation of itaconate and its derivatives reveals divergent inflammasome and type I interferon regulation in macrophages. Nat. Metab. *2*, 594–602.

36. Sun, K.A., Li, Y., Meliton, A.Y., Woods, P.S., Kimmig, L.M., Cetin-Atalay, R., Hamanaka, R.B., and Mutlu, G.M. (2020). Endogenous itaconate is not required for particulate matter-induced NRF2 expression or inflammatory response. Elife *9*, e54877.

37. Roth, D.B., and Flynn, H.W., Jr. (1997). Antibiotic selection in the treatment of endophthalmitis: the significance of drug combinations and synergy. Surv. Ophthalmol. *41*, 395–401.

38. Asbell, P.A., Sanfilippo, C.M., Sahm, D.F., and DeCory, H.H. (2020). Trends in antibiotic resistance among ocular microorganisms in the United States from 2009 to 2018. JAMA Ophthalmol., e200155.

39. Mills, E.L., Ryan, D.G., Prag, H.A., Dikovskaya, D., Menon, D., Zaslona, Z., Jedrychowski, M.P., Costa, A.S.H., Higgins, M., Hams, E., et al. (2018). Itaconate is an anti-inflammatory metabolite that activates Nrf2 via alkylation of KEAP1. Nature *556*, 113–117.

40. Tallab, R.T., and Stone, D.U. (2016). Corticosteroids as a therapy for bacterial keratitis: an evidence-based review of 'who, when and why'. Br. J. Ophthalmol. *100*, 731–735.

41. Ray, K.J., Srinivasan, M., Mascarenhas, J., Rajaraman, R., Ravindran, M., Glidden, D.V., Oldenburg, C.E., Sun, C.Q., Zegans, M.E., McLeod, S.D., et al. (2014). Early addition of topical corticosteroids in the treatment of bacterial keratitis. JAMA Ophthalmol. *132*, 737–741.

42. Cohen, E.J. (2009). The case against the use of steroids in the treatment of bacterial keratitis. Arch. Ophthalmol. *127*, 103–104.

43. Levy-Clarke, G., Jabs, D.A., Read, R.W., Rosenbaum, J.T., Vitale, A., and Van Gelder, R.N. (2014). Expert panel recommendations for the use of anti-tumor necrosis factor biologic agents in patients with ocular inflammatory disorders. Ophthalmology *121*, 785–96.e3.

44. O'Neill, L.A.J., and Artyomov, M.N. (2019). Itaconate: the poster child of metabolic reprogramming in macrophage function. Nat. Rev. Immunol. *19*, 273–281.

45. Basler, T., Jeckstadt, S., Valentin-Weigand, P., and Goethe, R. (2006). *Mycobacterium paratuberculosis*, *Mycobacterium smegmatis*, and lipopolysaccharide induce different transcriptional and post-transcriptional regulation of the *IRG1* gene in murine macrophages. J. Leukoc. Biol. *79*, 628–638.

46. Michelucci, A., Cordes, T., Ghelfi, J., Pailot, A., Reiling, N., Goldmann, O., Binz, T., Wegner, A., Tallam, A., Rausell, A., et al. (2013). Immune-responsive gene 1 protein links metabolism to immunity by catalyzing itaconic acid production. Proc. Natl. Acad. Sci. USA *110*, 7820–7825.

47. Juan, C., Torrens, G., Barceló, I.M., and Oliver, A. (2018). Interplay between peptidoglycan biology and virulence in Gram-negative pathogens. Microbiol. Mol. Biol. Rev. *82*, e00033-18.

48. Jamal Uddin, M., Joe, Y., Kim, S.K., Oh Jeong, S., Ryter, S.W., Pae, H.O., and Chung, H.T. (2016). IRG1 induced by heme oxygenase-1/carbon monoxide inhibits LPS-mediated sepsis and pro-inflammatory cytokine production. Cell. Mol. Immunol. *13*, 170–179.

49. Kochan, T., Singla, A., Tosi, J., and Kumar, A. (2012). Toll-like receptor 2 ligand pretreatment attenuates retinal microglial inflammatory response but enhances phagocytic activity toward *Staphylococcus aureus*. Infect. Immun. *80*, 2076–2088.

50. Nair, S., Huynh, J.P., Lampropoulou, V., Loginicheva, E., Esaulova, E., Gounder, A.P., Boon, A.C.M., Schwarzkopf, E.A., Bradstreet, T.R., Edelson, B.T., et al. (2018). *Irg1* expression in myeloid cells prevents immunopathology during *M. tuberculosis* infection. J. Exp. Med. *215*, 1035–1045.

51. Brockhaus, L., Goldblum, D., Eggenschwiler, L., Zimmerli, S., and Marzolini, C. (2019). Revisiting systemic treatment of bacterial endophthalmitis: a review of intravitreal penetration of systemic antibiotics. Clin. Microbiol. Infect. *25*, 1364–1369.

52. Periti, P., and Mazzei, T. (1998). Antibiotic-induced release of bacterial cell wall components in the pathogenesis of sepsis and septic shock: a review. J. Chemother. *10*, 427–448.

53. Lepper, P.M., Held, T.K., Schneider, E.M., Bölke, E., Gerlach, H., and Trautmann, M. (2002). Clinical implications of antibiotic-induced endotoxin release in septic shock. Intensive Care Med. *28*, 824–833.

54. Luan, H.H., and Medzhitov, R. (2016). Food fight: role of itaconate and other metabolites in antimicrobial defense. Cell Metab. *24*, 379–387.

55. Shamsuddin, N., and Kumar, A. (2011). TLR2 mediates the innate response of retinal Müller glia to Staphylococcus aureus. J. Immunol. *186*, 7089–7097.

56. Cordes, T., Wallace, M., Michelucci, A., Divakaruni, A.S., Sapcariu, S.C., Sousa, C., Koseki, H., Cabrales, P., Murphy, A.N., Hiller, K., and Metallo, C.M. (2016). Immunoresponsive gene 1 and itaconate inhibit succinate dehydrogenase to modulate intracellular succinate levels. J. Biol. Chem. *291*, 14274–14284.

57. Bambouskova, M., Gorvel, L., Lampropoulou, V., Sergushichev, A., Loginicheva, E., Johnson, K., Korenfeld, D., Mathyer, M.E., Kim, H., Huang, L.H., et al. (2018). Electrophilic properties of itaconate and derivatives regulate the IκBζ-ATF3 inflammatory axis. Nature *556*, 501–504.

58. Yi, Z., Deng, M., Scott, M.J., Fu, G., Loughran, P.A., Lei, Z., Li, S., Sun, P., Yang, C., Li, W., et al. (2020). Immune-responsive gene 1/itaconate activates nuclear factor erythroid 2-related factor 2 in hepatocytes to protect against liver ischemia-reperfusion injury. Hepatology *72*, 1394–1411.

59. Zheng, Y., Chen, Z., She, C., Lin, Y., Hong, Y., Shi, L., Zhang, Y., Cao, P., and Xu, X. (2020). Four-octyl itaconate activates Nrf2 cascade to protect osteoblasts from hydrogen peroxide-induced oxidative injury. Cell Death Dis. *11*, 772.

60. Hooftman, A., Angiari, S., Hester, S., Corcoran, S.E., Runtsch, M.C., Ling, C., Ruzek, M.C., Slivka, P.F., McGettrick, A.F., Banahan, K., et al. (2020). The immunomodulatory metabolite itaconate modifies NLRP3 and inhibits inflammasome activation. Cell Metab. *32*, 468–478.e7.

61. Kumar, A., Singh, P.K., Zhang, K., and Kumar, A. (2020). Toll-like receptor 2 (TLR2) engages endoplasmic reticulum stress sensor IRE1α to regulate retinal innate responses in Staphylococcus aureus endophthalmitis. FASEB J. *34*, 13826–13838.

62. Li, W., Cao, T., Luo, C., Cai, J., Zhou, X., Xiao, X., and Liu, S. (2020). Crosstalk between ER stress, NLRP3 inflammasome, and inflammation. Appl. Microbiol. Biotechnol. *104*, 6129–6140.

63. Menu, P., Mayor, A., Zhou, R., Tardivel, A., Ichijo, H., Mori, K., and Tschopp, J. (2012). ER stress activates the NLRP3 inflammasome via an UPR-independent pathway. Cell Death Dis. *3*, e261.

64. Capozzi, M.E., Giblin, M.J., and Penn, J.S. (2018). Palmitic acid induces Müller cell inflammation that is potentiated by co-treatment with glucose. Sci. Rep. *8*, 5459.

65. Fu, Z., Chen, C.T., Cagnone, G., Heckel, E., Sun, Y., Cakir, B., Tomita, Y., Huang, S., Li, Q., Britton, W., et al. (2019). Dyslipidemia in retinal metabolic disorders. EMBO Mol. Med. *11*, e10473.

66. Wen, H., Gris, D., Lei, Y., Jha, S., Zhang, L., Huang, M.T.-H., Brickey, W.J., and Ting, J.P.Y. (2011). Fatty acid-induced NLRP3-ASC inflammasome activation interferes with insulin signaling. Nat. Immunol. *12*, 408–415.

67. Riquelme, S.A., Liimatta, K., Wong Fok Lung, T., Fields, B., Ahn, D., Chen, D., Lozano, C., Sáenz, Y., Uhlemann, A.-C., Kahl, B.C., et al. (2020). *Pseudomonas aeruginosa* utilizes host-derived itaconate to redirect its metabolism to promote biofilm formation. Cell Metab. *31*, 1091–1106.e6.

68. Singh, P.K., Donovan, D.M., and Kumar, A. (2014). Intravitreal injection of the chimeric phage endolysin Ply187 protects mice from *Staphylococcus aureus* endophthalmitis. Antimicrob. Agents Chemother. *58*, 4621–4629.

69. Swamydas, M., and Lionakis, M.S. (2013). Isolation, purification and labeling of mouse bone marrow neutrophils for functional studies and adoptive transfer experiments. J. Vis. Exp. *10*, e50586.

70. Livak, K.J., and Schmittgen, T.D. (2001). Analysis of relative gene expression data using real-time quantitative PCR and the $2^{-\Delta\Delta C(T)}$ C_T method. Methods *25*, 402–408.

71. Chong, J., and Xia, J. (2018). MetaboAnalystR: an R package for flexible and reproducible analysis of metabolomics data. Bioinformatics *34*, 4313–4314.

72. Kuhl, C., Tautenhahn, R., Böttcher, C., Larson, T.R., and Neumann, S. (2012). CAMERA: an integrated strategy for compound spectra extraction and annotation of liquid chromatography/mass spectrometry data sets. Anal. Chem. *84*, 283–289.

73. Lê Cao, K.A., Boitard, S., and Besse, P. (2011). Sparse PLS discriminant analysis: biologically relevant feature selection and graphical displays for multiclass problems. BMC Bioinformatics *12*, 253.

74. Smith, C.A., Want, E.J., O'Maille, G., Abagyan, R., and Siuzdak, G. (2006). XCMS: processing mass spectrometry data for metabolite profiling using nonlinear peak alignment, matching, and identification. Anal. Chem. *78*, 779–787.

STAR★METHODS

KEY RESOURCES TABLE

REAGENT or RESOURCE	SOURCE	IDENTIFIER
Antibodies		
IRG1 (D6H2Y) Rabbit mAb	CST	77510S; RRID:AB_2799901
Anti-IRG1-Mouse	AvivaSysBio	ARP91387_P050
NRF2 (D1Z9C) XP (R) Rabbit mAb	CST	12721S; RRID:AB_2715528
HO-1 Rabbit mAb	CST	70081S; RRID:AB_2799772
NLRP-3 (D4D8T) Rabbit mAb	CST	15101S; RRID:AB_2722591
Caspase-1	Invitrogen	14-9832-82; RRID:AB_2016691
Chemicals, peptides, and recombinant proteins		
4-Octyl Itaconate	Gifted Dr. Luke O Neil	Trinity College Dublin, Scotland
Dimethyl itaconate	Sigma-Aldrich	109533-100G
Itaconic acid	Sigma-Aldrich	I29204-100G
Vancomycin	Cayman Chemicals	15327
TRIzol reagent	Life technologies	15596018
FBS (Fetal bovine serum)	CPS Serum	FBS-500-HI
Peptidoglycan (PGN)	Sigma-Aldrich	77140-10MG
Lipoteichoic acid (LTA)	Sigma-Aldrich	L2515-5MG
Alpha toxin (α-toxin)	Sigma-Aldrich	616385-250UG
Toxic shock syndrome toxin-1 (TSST1)	Sigma-Aldrich	T5662
Critical commercial assays		
Mice IL-1β ELISA kit	R&D System	DY401
Mice IL-6 ELISA kit	R&D System	DY406
Mice TNF-α ELISA kit	R&D System	DY410
Micro BCA Protein Assay Kit	Thermo Fisher Scientific	23235
SuperSignal West Femto Maximum Sensitivity Substrate	Thermo Fisher Scientific	34096
Maxima First Strand cDNA Synthesis Kit for RT-qPCR	Thermo Fisher Scientific	K1641
Radiant Green HiROX qPCR Kit	Alkali scientific	QS2050
Deposited data		
RNA sequencing data	NCBI	GEO: GSE168928
Experimental models: organisms/strains		
Mouse: C57BL/6J	The Jackson Laboratory	https://www.jax.org/strain/000664
Mouse: C57BL/6N-Acod1 $^{em1(IMPC)J}$/J (*Irg1*$^{-/-}$)	The Jackson Laboratory	https://www.jax.org/strain/029340
Mouse: B6.129X1-*Nfe2l2*^{tm1Ywk}/J	The Jackson Laboratory	https://www.jax.org/strain/017009
Software and algorithms		
Prism 8	GraphPad	https://www.graphpad.com
R version 3.6.3	R project	https://www.r-project.org/
MetaboAnalystR 3.0	Metaboanalyst	https://www.metaboanalyst.ca/
Other		
shRNA NRF-2	Santa Cruz	sc-37049-V

RESOURCE AVAILABILITY

Lead contact

Further information and requests for resources and reagents should be directed to and will be fulfilled by the Lead contact, Ashok Kumar (akuma@med.wayne.edu).

Materials availability

This study did not generate new unique reagents.

Data and code availability

The data generated from this study is deposited in the NIH Gene Expression Omnibus. The accession number for the raw and processed data is GSE168928.

EXPERIMENTAL MODEL AND SUBJECT DETAILS

Mice and ethics statement

Wild-type (WT) C57BL/6, *Nrf2*$^{-/-}$ and *Irg1*$^{-/-}$ mice (both male and female, aged 6-8 weeks) were purchased from the Jackson Laboratory and/or bred in-house in the Division of Laboratory Animal Resources facility at Kresge Eye Institute. Mice were maintained in a 12h light/dark cycle at 22°C and fed LabDiet rodent chow (Labdiet Pico lab Laboratory, St Louis, MO) and water *ad libitum*. All experimental procedures were performed in compliance with the Animals in Ophthalmic and Vision Research (ARVO) statement for the use of animals and were approved by the institutional animal care and use committee (IACUC) of Wayne State University.

Mouse model of bacterial endophthalmitis

Endophthalmitis was induced in WT, *Nrf2*$^{-/-}$ and *Irg1*$^{-/-}$ mice as described previously.[68] Briefly, mice were anesthetized and intravitreally injected with *S. aureus* RN6390 (5000 CFUs/eye in 2 μL volume) using a 32-G needle under an ophthalmoscope. Eyes injected with PBS served as controls. For treatment groups, itaconic acid (Sigma-Aldrich) or itaconate derivatives dimethyl itaconate (DMI, Sigma-Aldrich) or 4-octyl itaconate (OI) were injected intravitreally (10 μg/eye in 1μL volume) at 6 h post-infection.

Patient vitreous collection

A total of 22 patients clinically diagnosed and treated for infectious endophthalmitis (12 Gram-positive and 10 Gram-negative), who presented to the L V Prasad Eye Institute, Hyderabad, India, retina clinic and underwent diagnostic vitreous biopsy/vitrectomy between November 2018 and February 2019 were recruited for the study. Patient's demographical and clinical details are provided in the Table S1. In the control group, 10 patients with uninflamed eyes undergoing vitrectomy for non-infectious retinal disorders during the same period were included. In the test group, we excluded cases where the diagnosis was suspect or where the clinical characteristics were ambiguous. All patients diagnosed underwent complete ophthalmological examinations, including slit-lamp microscopy, visual acuity recordings, and later underwent pars plana vitrectomy. All cases were culture positive and had clinical features such as intense anterior chamber inflammation, extensive vitreous exudates, corneal infiltrates, or a lens abscess suggestive of infectious endophthalmitis. Written informed consent was obtained from all subjects and the study was approved by the Institutional Review Board, (LEC 09-18-125) L V Prasad Eye Institute, Hyderabad, India. The microbiological processing of the vitreous samples from the study group included direct microscopy and culture. A small portion of the vitreous sample (~100μL) was immediately stored at −80°C for itaconate measurement.

Cell and culture conditions

The immortalized human Müller glia cell line MIO-M1 was cultured in DMEM at 37°C in 5% CO2 supplemented with 10% FBS, 1% penicillin-streptomycin and 10 μg/mL L-glutamine. Prior to infection cells were grown overnight in serum and antibiotic-free media and infected with *S. aureus* (MOI, 10:1) for various time points.

METHOD DETAILS

Bacterial burden estimation

Mouse eyes were enucleated following infection and 24h post-drug treatment. Whole-eye lysates were prepared in 250 μL of PBS by homogenization using stainless steel beads in a tissue lyser (QIAGEN, Valencia, CA). A small portion (50 μL) of the tissue homogenate was serially diluted and plated on Tryptic Soy Agar (TSA) to enumerate bacterial burden. The following day, colonies were counted, and results were expressed as the mean number of CFUs/eye ± SD.

Isolation of bone marrow-derived macrophages

Mouse bone marrow-derived macrophages (BMDMs) were isolated as described previously.[14,69] Briefly, mice were euthanized, and bone marrow was flushed from tibias and femurs with RPMI media containing 10% FBS and 0.2 mM EDTA. Cells were pelleted by centrifugation at 400 x g for 5 minutes at 4°C. Red blood cells (RBCs) were lysed by adding 0.2% NaCl solution for 20-30 s, followed by the addition of 1.6% NaCl and centrifugation. Following RBC lysis, cell pellets were washed with RPMI media by centrifugation. Cells were re-suspended and seeded in RPMI media supplemented with 10% FBS, 100 U/ml penicillin, 100 mg/mL streptomycin and 10 ng/ml M-CSF for macrophage differentiation at 37°C in 5% CO_2. Six days post differentiation 4 × 10^6 BMDMs/mL were seeded in 65 mm Petri-dishes for *in vitro* experiments. For drug treatments, BMDMs were pretreated with DMI or OI (125 μM) for 2 h followed by challenge with *S. aureus* (multiplicity of infection (MOI) 10:1), for 8h.

Determination of the minimum inhibitory concentration (MIC)

A micro broth-dilution method was used to determine the MIC for vancomycin, OI, and DMI as described previously.[68] Briefly, bacterial cultures (10^5 CFU/well) were exposed to a two-fold serial dilution of the test compound in a 96-well plate. Following overnight incubation, the optical density (A_{600}) of each microplate well was recorded using a spectrophotometer. MICs were determined based on the optical density of the growth in control and the lowest vancomycin, DMI, or OI concentrations that resulted in *S. aureus* growth inhibition compared with media alone.

RNA extraction and real-time PCR

Mouse neural retinas were removed and pooled (two retinas per sample) in Trizol for RNA isolation. Total RNA was extracted from the retina as per the manufacturer's instructions (Thermo Scientific, Rockford, IL). RNA was reversed transcribed using a Maxima first-strand cDNA synthesis kit as per the manufacturer's protocol (Thermo Scientific, Rockford, IL). Quantitative assessment of gene expression was carried out by quantitative real-time PCR (qPCR) using gene-specific primers on a StepOne Plus Real-Time PCR System (Applied Biosystems, Foster City, CA, USA). The data were analyzed using the comparative $\Delta\Delta C_T$ method as described previously.[70] The gene expression in the test samples was normalized to endogenous β-actin controls.

Histology

Following infection and drug treatment, eyes were enucleated and fixed in 4% formalin for histopathological examination. The embedding, sectioning, and hematoxylin & eosin (H&E) staining was performed by Excalibur Pathology, Inc. (Oklahoma City, OK, USA). Pathscan Enabler IV (Meyer Instruments, Inc.) was used to scan H&E stained slides.

Cytokine ELISA

For *in vivo* samples, eyes were enucleated, and lysates were prepared by homogenization using a tissue lyser as described above. The tissue homogenates were centrifuged at 15,000 x g for 20 minutes at 4°C and the clear supernatants were used to estimate cytokine concentration. For *in vitro* studies, the conditioned media from *S. aureus*-infected and drug-treated groups along with vehicle control were used for cytokine measurements. ELISA for inflammatory cytokines IL-1β, IL-6, and TNF-α was performed as per the manufacturer's instructions (R&D System, Minneapolis, USA).

Measurement of intracellular reactive oxygen species (ROS)

ROS production was measured by fluorescence microscopy using dichloro-dihydrofluorescein diacetate (DCFH-DA) as described previously.[34] Briefly, BMDMs were grown in a 4-well chamber slide and infected with *S. aureus* (MOI, 10:1) for 4h. Following infection, cells were washed with PBS and incubated with 10 μM of DCFH-DA for 30min at 37°C. The cells were then washed twice with PBS and observed via an Eclipse 90i fluorescence microscope (Nikon).

shRNA mediated knockdown

The lentiviral particles containing scrambled control shRNA, NRF2 shRNA (sc-37049-V) were purchased from Santa Cruz Biotechnology (Dallas, TX). The shRNA knockdowns were performed as per the manufacturer's protocol. The knockdown of target proteins was confirmed by western blotting. The conditioned media were preserved for cytokine ELISA.

Western blotting

Protein samples from BMDMs and Müller glia (MIO-M1) cells were prepared by direct lysis of cells in radioimmunoprecipitation assay (RIPA) buffer containing protease and phosphatase inhibitor cocktails. For *in vivo* samples, two neuroretina (without RPE and choroid) were pooled in RIPA buffer, and homogenates were prepared using sonication followed by centrifugation at 15,000 x g for 20min at 4°C. The total protein concentration of the cell and retinal lysates were determined using a Micro BCA protein assay kit (Thermo Scientific, Rockford, IL). Protein samples (30-40 μg) were resolved on SDS–PAGE (8%–10%) and transferred onto a nitrocellulose membrane (0.45 μm) using a wet transfer system. Membranes were blocked in 5% (w/v) dried milk in tris-buffered saline (TBS)-Tween (TBST) for 1h at room temperature. Membranes were incubated with primary antibodies: anti-NRF2, anti-Hem-oxygenase 1 (HO-1), anti-NLRP-3, anti-HSP-90, (Cell Signaling Technology), anti-IRG1 (Aviva Bio-system), anti-Caspase-1 (Santa Cruz Biotechnology), as per the manufacturer's instructions and followed by the appropriate anti-mouse/rabbit horseradish peroxidase (HRP)-conjugated secondary antibody. To visualize the protein bands, the membranes were exposed to Super signal West Femto chemiluminescent substrate (Thermo-scientific, Rockford, IL). For semiquantitative analysis, immunodetected protein band intensities were measured using ImageJ software (Rasband, W.S., ImageJ, U.S. National Institutes of Health, Bethesda, Maryland, http://rsb.info.nih.gov/ij/, 1997–2009).

Liquid chromatography coupled with a tandem mass spectrometer (LC-MS/MS)

Itaconate levels in the mouse retina/vitreous and cultured murine BMDMs were measured by LC-MS/MS methods at the Pharmacology and Metabolomics Core, Karmanos Cancer Institute, Wayne State University. Briefly, cell pellets were re-suspended in 1 mL of 80% MeOH (cooled in an ice bath), sonicated with a Misonix XL-2000 probe sonicator, and centrifuged at 28,672 x g for 10min at 4°C. The supernatant was transferred into a new 2 mL centrifuge tube. The pellet was washed with 200 μL of 80%

MeOH (ice bath) by vortexing thoroughly and centrifuged at 28,672 x g for 10min at 4°C. Supernatant from two rounds of extraction was combined and dried in a CentriVap Refrigerated Centrifugal Concentrator. The residue was reconstituted with 50 μL of ddH_2O, and a series of 20-time dilution samples were prepared for paralleled quantification by Waters Acquity H-class UPLC system connected to a Xevo TQ-xS triple LC-MS/MS system. The itaconate levels in the patient vitreous were measured by LC-MS/MS as indicated above at the Indian Institute of Chemical Technology, Hyderabad, India.

Preprocessing and annotation of metabolomic and transcriptomic data

The metabolomics raw data were acquired from LC-QTOF/MS and were converted to a mzData format using Mass Hunter Qualitative Analysis Software (Agilent) and then imported to xcms R package for preprocessing. The default parameters in xcms software were used. The preprocessed data were obtained with three features of the dataset, including the retention time, the mass-to-charge ratio (m/z), and peak intensity.[71] The annotation was done using the CAMERA R package to annotate isotope peaks, adducts, and fragments.[72] Lastly, the data were normalized for each sample as described in the statistical analysis section.

For transcriptomic data analysis, the original Affymetrix data was pre-processed using an oligo R package and later normalized and log-transformed using a multi-array average (RMA) method. Further, the CDF package was used for probe annotation of Affymetrix data. The probes of the normalized data were successfully mapped to Entrez Gene IDs and Gene Symbols by annotation package (annotate) in R. Wherever multiple probes matched a single gene symbol, we calculated the median values of those probes as the expression value for that gene.

Metabolomic and transcriptomic data analysis

Multivariate data analysis of Metabolomics data was performed using MetaboAnalyst R package.[73] Identification of clusters to locate metabolites across various time points was performed using a supervised partial least-squares discriminant analysis (PLS-DA) method.[74] The metabolites were ranked for PC1 and PC2, and in an absence of internal validation, the PLS-DA method avoided overfitting of metabolites. The PLS-DA found differences in metabolites between the various time points versus controls. Variable importance was calculated as a coefficient for the selection of each variable. In addition to the supervised method, the nonparametric Kruskal–Wallis test was also performed to measure the importance of each metabolite. The R package "caret" was used for the random forest method to classify key altered metabolites. All default values of the caret package were used. The top metabolites were obtained based on the "Gini" score ranking. For Affymetrix gene expression data, all statistical analyses were performed using the multiple R Bioconductor packages (http://www.Bioconductor.org). For analysis, the *P*-values were adjusted for multiple testing with the Benjamini and Hochberg's method to control for false discovery rate (FDR). Probe sets showing at least a ± 2.5-fold change and an FDR < 0.05 were considered significant for the analysis. ggplot2 was used to generate the plots, R package VennDigram was used to generate the Venn diagram and the heatmap.2 package was used for heatmap generation from fold changes value.

QUANTIFICATION AND STATISTICAL ANALYSIS

Statistical analyses were performed using Prism version 8.1 (Graph Pad, San Diego, CA). Data were expressed as mean ± SD unless indicated otherwise and statistical significance was determined using either unpaired Student's t test or two-way ANOVA or one-way ANOVA with multiple comparisons as indicated in the figure legends. A confidence interval of 95% was used for all statistical tests. A $p < 0.05$ was considered statistically significant.